Sloshing in a rotating liquid inside a closed sea cage for fish farming

Andrei Tsarau,[1] Claudio Lugni,[2,3,4,a)] Alessia Lucarelli,[3] David Kristiansen,[5] and Pål Lader[5]

[1)] *SINTEF Ocean, Trondheim, Norway*

[2)] *Institute of Marine Hydrodynamics, Harbin Engineering University, Harbin, China*

[3)] *CNR-INM, Marine Technology Research Institute, Rome, Italy*

[4)] *NTNU-AMOS, Center for Autonomous Marine Operation Systems, Trondheim, Norway*

[5)] *NTNU, Department of Marine Technology, Trondheim, Norway*

(Dated: 29 December 2020)

Sloshing in a sea cage with a slowly rotating liquid is investigated. The cage is axisymmetric, and the liquid is subjected to a nearly uniform angular velocity about the vertical axis of the cage. Both experimental and theoretical investigations are presented. It is shown that rotation modifies the sloshing regimes of the non-rotating liquid by splitting the natural frequencies. Therefore, resonant sloshing regimes can be manipulated by varying the rotation rate of the liquid.

[a)] claudio.lugni@cnr.it, corresponding author

I. INTRODUCTION

The development of closed containment systems for sea-based fish farming has been prompted by the increased problems due to sea lice and the negative environmental impact, which are often associated with open aquaculture systems (net pens). By enclosing the production volume, the risk of sea-lice infections and the need for medical treatment can be reduced, and wastes can be safely collected for recycling. Furthermore, the production efficiency can be improved by optimizing parameters such as water temperature, oxygen saturation, and acidity. These advantages of closed cages, compared to the traditional net pens, can potentially improve fish welfare and reduce the environmental impact of marine fish farming in general. Studies show that the use of deep see water in the closed cages can provide sufficient protection against sea lice[1]. For this, however, the water must be continuously exchanged and circulated through the cage, which is typically enabled by a hydraulic circulation system consisting of compressors, water pipes, inlets and outlets. Moreover, adequate water-flow conditions in culture cages are vital for fish growth and welfare (e.g., Hvas et al. 2020[2]). Therefore, e.g., in circular (axisymmetric) closed cages for salmon production, a water current is artificially maintained by the circulation system forcing the contained water to move in a circular pattern – rotating flow.

Ocean waves may excite free surface oscillation of the liquid inside the floating cage causing sloshing. Sloshing is the resonance of the fluid in a partially filled tank which causes large response, i.e. large free-surface deformation, even for small amplitude of the forcing motion. For engineering applications, it matters when the excitation frequency is close to the lowest natural frequency of the liquid motion. This is relevant for the resonant free-surface motion of the fuel in the tank of missiles, rockets and airplanes[3] possibly causing dynamic instability, or for the violent liquid motion in the tank of a ship carrier, which could affect the structural integrity of the tank (e.g. oil carrier, LNG ship), both due to the large local hydrodynamic loads on the tank wall[4,5] and the possible local hydroelastic effects[6]. Sloshing flows have been widely studied in the past, in relation with the filling depth of the tank which governs the natural frequency of the liquid motion, both for two-dimensional (Bouscasse et al, 2013[7], in shallow water condition; Faltinsen et al, 2000[8], in finite water depth) and three-dimensional[9] ship prismatic tank. A comprehensive literature review can be found in Malenica et al. (2017)[5] in particular for the sloshing flows in LNG ship carri-

ers. The literature about the sloshing flows in cylindrical tank is less intensive. Generally, when a three-dimensional tank is considered, both prismatic or cylindrical shaped, swirling wave motion occurs as a consequence of the solution bifurcation at a forcing frequency close to the natural frequency[10,11]. Three bifurcation points can be identified, which bound the frequency ranges where stable planar, swirling and irregular waves occur[12]. A "...highly three-dimensional behaviour of the free surface and a rotational effect ..." was also experimentally observed by Caron et al.(2018)[13] near the resonance frequency region for several water depths. The behaviour was confirmed by the same authors through an accurate numerical study. By using the multimodal method, Faltinsen et al. (2016)[12] investigated for the first time, a combined surge-sway-pitch-roll tank motion leading to an elliptic and longitudinal forcing. They concluded that when a rotary forcing is provided, the irregular wave frequency range vanishes and co-directed (with the forcing) swirling waves cover the whole primary resonance frequency region.

For the specific application related to the closed fish cage, sloshing may interact with the internal flow and thus lead to complex hydrodynamic effects. Although different designs of closed systems exist, e.g., raceways, we will consider only axisymmetric cages in which the liquid flow is rotating around the vertical axis of the cage. For such cages, sloshing will occur in a rotating liquid. As a result of, e.g., Coriolis effects, the characteristics of resonant sloshing in a rotating liquid can be quite different from the resonant motions in a non-rotating liquid[14–16]. From an aquaculture engineering perspective, these hydrodynamic effects may represent a significant challenge as they cannot be modelled or predicted using conventional methods for structural or hydrodynamic analysis. In the scientific literature, similar problems (fluid dynamic behaviour in spinning tanks) have been found only in the studies of stability and control of rockets, space vehicles, liquid-cooled gas turbines and centrifuges[17]; however, it is not straightforward to apply the results of these studies to aquaculture tanks. From a marine technology perspective, a closed fish cage represents a large volume structure, and most of its volume is occupied by a liquid. Considering the huge mass of the contained liquid, its motion can exert significant loads on the cage and may affect its stability. This is very important for the design of closed cages. Furthermore, to ensure the well-being of the produced fish, it is essential to maintain a favourable environment in the cage, which would mainly depend on the quality of the contained water, its velocities and accelerations. The latter parameters are also directly related to the cage's internal hydrodynamics, em-

phasizing its importance for closed fish-farming systems. Thus, the problems of internal hydrodynamics, including free-surface effects, rotating flows and their interaction with the structural elements, are important design considerations for floating closed cages. However, the knowledge on and experience with these problems are quite limited, as offshore fish farming in closed cages is still a novel concept. Some few research studies on the behaviour of such structures in the marine environment are found in Strand and Faltinsen (2019)[18], Tan et al. (2019)[19], Strand (2018)[20], Kristiansen et al. (2018)[21], Lader et al. (2017)[22] and Lader et al.(2015)[23]. These authors focused on the seakeeping behaviour of various closed-cage concepts, considering sloshing but neglecting the presence of rotation in the contained liquid. The latter may be a serious limitation of these studies. In this paper, we present a unique study on sloshing in an aquaculture closed-containment system with a slowly rotating liquid. In contrast to the previous studies, the effect of rotation on the fundamental sloshing modes is considered in detail, whereas the presence of fish is neglected. This study also concerns amplitudes of sloshing waves, their damping and possible suppression due to rotation and the overall effect of sloshing on the hydrodynamic loads on a circular-cylindrical tank undergoing forced motion. Both laboratory experiments with a scaled physical model and a numerical analysis are presented. Two theories were used in the analysis: a weakly nonlinear multimodal theory for sloshing in a non-rotating liquid[24] and a linear theory for a rotating liquid[15].

II. THEORETICAL BACKGROUND AND NUMERICAL MODELS

A. Assumptions

We consider a closed cage to be a vertical, cylindrical tank of radius R, and the liquid depth inside the tank to be h. For the non-rotating liquid, we adopt a model based on the infinite-dimensional nonlinear modal theory for liquid sloshing dynamics by Faltinsen and Timokha (2009)[24]. Following the original formulation, the modal equations and the equations of the tank motion are expressed in the tank-fixed coordinate system (Figure 1). The tank is rigid, and it is partially filled with an inviscid incompressible liquid. The range of possible liquid-depth-to-tank-radius ratios (h/R) is between 0.2 to 3.0. In general, any unsteady velocity of the tank can be modelled; however, in our case, only small motions

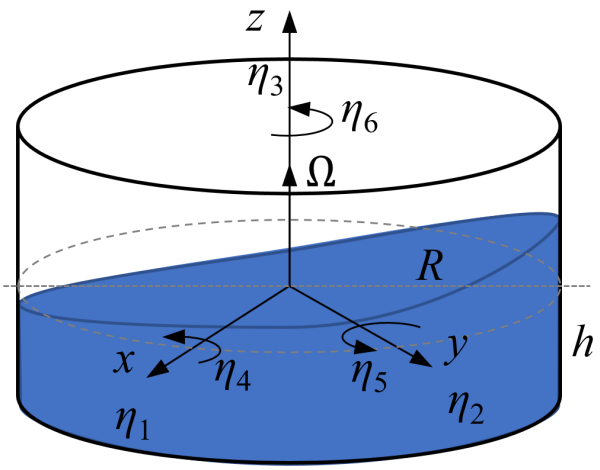

FIG. 1. Coordinate systems of the closed cage centered at the equilibrium free surface.

of the tank are considered, and therefore in the absence of rotation, the tank coordinates (η_1, η_2, η_3) can be considered equivalent to the fixed coordinates (x, y, z). If the liquid is subjected to a uniform angular velocity Ω about the z axis, the free oscillations of the liquid can be modelled in linear approximation in a coordinate system rotating with the liquid[15]. To use the latter approach in our application, we assumed that equilibrium velocities of the liquid in the circular cage can be approximated by a distribution corresponding to a rigid-body rotation. This assumption was made based on the experimental results by Plew et al. (2015)[25], who measured mean flow velocities (driven by the inflow from the water supply system) in a circular aquaculture tank with juvenile Atlantic salmon inside. The measured profiles of tangential velocity were nearly linear and depth-independent, resembling a rigid-body rotation and thus supporting our assumption. Note, however, that assuming the liquid to rotate as a rigid body is only an approximation of the true velocity field, which in reality may have a very complex structure.

Finally, we limit our analysis to rotation rates Ω that are less than half the sloshing frequency (i.e., a slowly rotating liquid). The reason for this condition will be explained in Section II C 1; however, it does not seem to lead to any serious limitation in the analysis of typical circular closed cages. For the latter, we can simply require $\Omega < (g/R)^{0.5}$, where g is the acceleration of gravity. For fish welfare, the maximum velocity in the cage ($U_{max} = R\Omega$) should be limited by the critical swimming speed (i.e., the maximum velocity that can be maintained by a fish for a specific period of time), which usually does not exceed 1 m/s for

Atlantic salmon[2]. Thus, the liquid rotation rate in aquaculture cages is relatively low.

B. Modal approach for a non-rotating liquid

1. *Natural sloshing modes*

Following modal theory, the tank free-surface elevation ξ is expanded as a series in terms of so-called natural sloshing modes $\chi_{m,i,k}(x,y)$:

$$\xi(x,y,t) = \sum_{m,i,k} \beta_{m,i,k}\,(t)\,\chi_{m,i,k}(x,y) \tag{1}$$

where $\beta_{m,i,k}$ are the generalized coordinates for liquid motion, which are infinite in number, and the sum goes over all β. According to linear potential flow theory, the natural modes for an upright circular cylinder in a cylindrical coordinate system (r,θ,z) can be expressed as

$$\chi_{m,i,k}(x,y) = \chi_{m,i,k}(rcos\theta, rsin\theta) = \frac{J_m(l_{m,i}r/R)}{J_m(l_{m,i})} \times \begin{Bmatrix} \cos(m\theta) \\ \sin(m\theta) \end{Bmatrix} \tag{2}$$

where J_m is the Bessel function of the first kind of order m, and $l_{m,i}$ are the nondimensional roots of the equation $J_m{}'\,(l_{m,i}) = 0$, and index k (= 1 or 2) corresponds to the cosine or sine mode terms, respectively. For each natural mode, the corresponding natural frequencies are

$$\sigma_{m,i}^2 = \frac{g}{R} l_{m,i} \tanh(l_{m,i}\frac{h}{R}) \tag{3}$$

Here, g is the acceleration of gravity (9.81 m/s^2), and m = 0, 1 ..., i =1, 2, ... are the so-called azimuthal and radial mode numbers, respectively.

2. *Modal equations for prescribed tank motions*

When rigid-body motions η_i are known, the following ordinary differential equations approximates liquid motion in terms of the generalized coordinates:

$$\ddot{\beta}_{1,j,1} + \sigma_{1,j}^2\beta_{1,j,1} + 2\sigma_{1,j}\delta_{1,j}\dot{\beta}_{1,j} + B_{1,j,1} = -P_j\,[\ddot{\eta}_1 - g\eta_5 - S_j\ddot{\eta}_5] \tag{4}$$

$$\ddot{\beta}_{1,j,2} + \sigma_{1,j}^2\beta_{1,j,2} + 2\sigma_{1,j}\delta_{1,j}\dot{\beta}_{1,j} + B_{1,j,2} = -P_j\,[\ddot{\eta}_2 + g\eta_4 + S_j\ddot{\eta}_4] \tag{5}$$

$$\ddot{\beta}_{2,j,k} + \sigma_{2,j}^2\beta_{2,j,k} + 2\sigma_{2,j}\delta_{2,j}\dot{\beta}_{2,j} + B_{2,j,k} = 0 \qquad k = 1,2 \tag{6}$$

$$\ddot{\beta}_{0,j,1} + \sigma_{0,j}^2 \beta_{0,j,1} + 2\sigma_{0,j}\delta_{0,j}\dot{\beta}_{0,j,1} + B_{0,j,1} = 0 \tag{7}$$

$$P_j = \frac{2l_{1,j}\tanh\left(l_{1,j}h/R\right)}{l_{1,j}^2 - 1} \tag{8}$$

$$S_j = \frac{2R\tanh\left(l_{1,j}h/2R\right)}{l_{1,j}} \tag{9}$$

In this approximation, $j = 1, 2, \ldots \leq I_r$ (number of the radial modes), $m = 0, 1, 2$ – the only azimuthal numbers that may have a nonzero contribution, and $B_{m,j,k}$ are the nonlinear terms defined below. The linear damping term (with modal damping ratios denoted by $\delta_{m,j}$) is introduced artificially in order to achieve steady-state solutions of the modal equations. Possible values of $\delta_{m,j}$ are discussed in Section II B 3.

The nonlinear terms in the above modal equations are derived by Faltinsen and Timokha (2009)[24] for tank excitation frequencies close to $\sigma_{1,1}$. Following the traditional notations, $p_1 = \beta_{1,1,1,}, r_1 = \beta_{1,1,2}$, $p_0 = \beta_{0,1,1}$, $p_2 = \beta_{2,1,1}$, $r_2 = \beta_{2,1,2}$, the nonlinear terms read:

$$\begin{aligned} B_{1,1,1} =& \frac{d_1}{R^2} p_1 \left(p_1\ddot{p}_1 + \dot{p}_1^2 + r_1\ddot{r}_1 + \dot{r}_1^2\right) + \\ & \frac{d_2}{R^2}\left(r_1^2\ddot{p}_1 + 2r_1\dot{r}_1\dot{p}_1 - r_1p_1\ddot{r}_1 - 2p_1\dot{r}_1^2\right) + \\ & \frac{d_3}{R}\left(p_2\ddot{p}_1 + r_2\ddot{r}_1 + \dot{r}_1\dot{r}_2 + \dot{p}_1\dot{p}_2\right) - \\ & \frac{d_4}{R}\left(p_1\ddot{p}_2 + r_1\ddot{r}_2\right) + \frac{d_5}{R}\left(p_0\ddot{p}_1 + \dot{p}_1\dot{p}_0\right) + \frac{d_6}{R}p_1\ddot{p}_0 \end{aligned} \tag{10}$$

$$\begin{aligned} B_{1,1,2} =& \frac{d_1}{R^2} r_1 \left(r_1\ddot{r}_1 + \dot{r}_1^2 + p_1\ddot{p}_1 + \dot{p}_{1^2}\right) + \\ & \frac{d_2}{R^2}\left(p_{1^2}\ddot{p}_1 + 2p_1\dot{r}_1\dot{p}_1 - r_1p_1\ddot{p}_1 - 2r_1\dot{p}_{1^2}\right) - \\ & \frac{d_3}{R}\left(p_2\ddot{r}_1 + r_2\ddot{p}_1 + \dot{r}_1\dot{p}_2 - \dot{p}_1\dot{r}_2\right) + \\ & \frac{d_4}{R}\left(r_1\ddot{p}_2 - p_1\ddot{r}_2\right) + \frac{d_5}{R}\left(p_0\ddot{r}_1 + \dot{r}_1\dot{p}_0\right) + \frac{d_6}{R}r_1\ddot{p}_0 \end{aligned} \tag{11}$$

$$B_{0,1,1} = \frac{d_{10}}{R}\left(r_1\ddot{r}_1 + p_1\ddot{p}_1\right) + \frac{d_8}{R}\left(\dot{r}_1^2 + \dot{p}_1^2\right) \tag{12}$$

$$B_{2,1,1} = \frac{d_9}{R}\left(r_1\ddot{r}_1 - p_1\ddot{p}_1\right) + \frac{d_7}{R}\left(\dot{r}_1^2 - \dot{p}_1^2\right) \tag{13}$$

$$B_{2,1,2} = \frac{d_9}{R}\left(r_1\ddot{p}_1 + p_1\ddot{r}_1\right) - \frac{2d_7}{R}\dot{r}_1\dot{p}_1 \tag{14}$$

The nondimensional coefficients $d_1, \ldots\ d_{10}$ in these nonlinear terms are tabulated by Faltinsen and Timokha (2009)[24] for a range of h/R between 0.2 to 3.0. The presented model includes nonlinear terms only for the two primary excited modes ($(1,1,1)$ and $(1,1,2)$) and

the secondary modes $((0,1,1),(2,1,1),(2,1,2))$. Thus, there is no coupling between the third-order modes and higher.

3. Viscous energy dissipation

Although potential theory assumes inviscid liquid, viscous energy dissipation in the liquid can be included in the modal equations for liquid motion, as shown in the previous section. In general, there is viscous dissipation in both the boundary layers and in the bulk. However, bulk dumping is often considered small relative to boundary-layer damping and is usually neglected[24]. Royon-Lebeaud et al. (2007)[11] have shown that for dissipation at the boundaries of a circular-cylindrical tank, the damping ratios can be estimated using the following analytical expression:

$$\delta_{m,n} = \frac{1}{2R}\left(\frac{\nu}{2\sigma_{m,n}}\right)^{1/2}\left[\frac{2l_{m,n}}{sinh(2l_{m,n}h/R)} + \frac{2l_{m,n}cosh^2(l_{m,n}h/R)}{sinh(2l_{m,n}h/R)} + \frac{1+(m/l_{m,n})^2}{1-(m/l_{m,n})^2} - \frac{2l_{m,n}h/R}{sinh(2l_{m,n}h/R)}\right] \tag{15}$$

where ν is the kinematic viscosity of the liquid. Note, however, that Royon-Lebeaud et al. (2007)[11] used this expression for smooth-wall cylinders with radii up to 0.15 m. We use this expression in Eqs. (4) - (7) and will investigate whether it can also be applicable for a larger cylindrical cage equipped with a pipe system generating a rotating flow inside the cage (as in our experiment).

4. Hydrodynamic force

The total hydrodynamic force on the tank can be expressed via the generalized coordinates following Faltinsen and Timokha (2009)[24]:

$$F_{\eta_1} = \pi\rho R^2 h(g\eta_5 - \ddot{\eta}_1 + \frac{1}{2}h\ddot{\eta}_5) - \sum_{j=1}^{I_r}\frac{\pi\rho R^3}{l_{1,j}^2}\ddot{\beta}_{1,j,1} \tag{16}$$

$$F_{\eta_2} = \pi\rho R^2 h(-g\eta_4 - \ddot{\eta}_2 + \frac{1}{2}h\ddot{\eta}_4) - \sum_{j=1}^{I_r}\frac{\pi\rho R^3}{l_{1,j}^2}\ddot{\beta}_{1,j,2} \tag{17}$$

$$F_{\eta_3} = -\pi\rho R^2 h(g + \ddot{\eta}_3) \tag{18}$$

where ρ is the liquid density. The hydrodynamic moment can also be expressed via the generalized coordinates in the same manner. However, its expression becomes lengthy due to the introduction of so-called Joukowsky inertial tensor, which is different from the inertia tensor of a solid, but can be expressed analytically for a cylindrical tank (e.g., Faltinsen and Timokha 2009[24]).

C. Linear theory for sloshing in a rotating liquid

1. Governing equations

In this section, we consider free oscillations of a rotating liquid in a circular tank under the assumption that the equilibrium motion of the liquid be a rigid-body rotation (as explained in Section II A). Resonant oscillatory motions superimposed on the liquid rotation can exert extremely large forces on the tank. For that reason, the natural frequencies of the rotating liquid are of much interest, and a method to calculate them is presented here. This method follows from the mathematical model for linear oscillations of a liquid in a vertical, rotating, circular cylinder developed by Miles (1959)[15].

For the liquid subjected to a uniform angular velocity Ω about the z axis, the governing equations of small motion can be expressed in a fairly simple way if the liquid velocity ($\mathbf{q}$) is measured relative to a set of axes rotating with Ω about z (Figure 1). In this case, the Euler equation for an inviscid liquid in a rotating polar coordinate system (r, θ, z), when nonlinear terms are neglected, reads as[15]:

$$\frac{\partial \mathbf{q}}{\partial t} + 2\mathbf{\Omega} \times \mathbf{q} + \mathbf{\Omega} \times (\mathbf{\Omega} \times \mathbf{r}) = -\nabla \left(\frac{p}{\rho} + gz \right) \tag{19}$$

where the radius vector $\mathbf{r}$ is perpendicular to the spin axis z, i.e., $\mathbf{\Omega} = (0, 0, \Omega)$. This equation is simplified further by introducing the acceleration potential:

$$\psi = \frac{p}{\rho} + gz - \frac{1}{2}\Omega^2 r^2$$

which specifies the pressure in excess of the steady state pressure caused by the centrifugal and gravitational force fields. The free surface shape ξ is therefore defined by the condition $\psi = 0$ and $p = 0$.

The fluid motions are assumed to be harmonic in time with a frequency σ (i.e., $\mathbf{q}\ exp(i\sigma t)$); hence the time derivative $\frac{\partial \mathbf{q}}{\partial t}$ can be replaced by $i\sigma\mathbf{q}(r, \theta, z)$, where now $\mathbf{q}$ is the spatial part

of the velocity. With these definitions and assumptions and using the fact that the liquid is incompressible ($\nabla \cdot \mathbf{q} = 0$), the following differential equation is derived by taking the divergence of the above Euler equation and differentiating twice with respect to time[14]:

$$\frac{1}{r}\frac{\partial}{\partial r}\left(r\frac{\partial \psi}{\partial r}\right) + \frac{1}{r^2}\frac{\partial^2 \psi}{\partial \theta^2} + \left[1 - \left(\frac{2\Omega}{\sigma}\right)^2\right]\frac{\partial^2 \psi}{\partial z^2} = 0 \tag{20}$$

where ψ is now defined as only the spatial part of the acceleration potential. The solutions of this equation must satisfy boundary conditions at the tank walls and bottom (velocity perpendicular to the wall is zero) and at the free surface. The latter reads

$$g\frac{\partial \psi}{\partial z} - \sigma^2 \psi = 0 \tag{21}$$

and is to be satisfied at $z = 0$.

The differential equation Eq. (20) is elliptic when $\sigma > 2\Omega$, and therefore we may expect the associated solution to be qualitatively similar to its counterpart for $\Omega = 0$, i.e., sloshing of a non-rotating liquid. It is reasonable to assume $\sigma > 2\Omega$ for typical aquaculture tanks, hence only this case is considered. A suitable set of elementary solutions to Eq. (20) is given by Miles (1959)[15]:

$$\Psi = e^{i(\sigma t + m\theta) + \kappa z} J_m(kr) \tag{22}$$

where m is any integer, k is to be determined, and $\kappa = k/\sqrt{\left[1 - \left(\frac{2\Omega}{\sigma}\right)^2\right]}$. The corresponding radial velocity (the radial component of $\mathbf{q}$) is given by

$$u = \frac{\partial \Psi}{\partial r} + m\frac{2\Omega}{\sigma}\frac{\Psi}{r} \tag{23}$$

and there are similar expressions for the tangential and axial velocity components.

The construction of more general solutions from those of Ψ leads naturally to orthogonal expansions in $J_m(kr)$ for those eigenvalues of k, say k_n, determined by

$$\frac{\partial J_m}{\partial r}(x) + m\frac{2\Omega}{\sigma}\frac{J_m(x)}{x} = 0 \qquad x = k_n R \tag{24}$$

corresponding to $u = 0$ at $r = R$. An alternative form of this expression, more suitable for determining the natural frequencies, is

$$(\lambda - 1) J_{|m|-1}(x) + (\lambda + 1) J_{|m|+1}(x) = 0 \tag{25}$$

where $\lambda = \frac{-2\Omega}{\sigma}\,\mathrm{sign}(m)$.

Now, we outline a method to determine the natural frequencies for sloshing in a rotating

liquid. We seek those values of λ (and corresponding σ) which satisfy both Eq. (25) and the free surface condition Eq.(21). If the tank is assumed to be sufficiently deep (say depth $>$ diameter) to permit the approximation $\tanh(\kappa h) \approx 1$, the elementary solutions Ψ satisfy Eq. (21) individually. This additional assumption simplifies our analysis; however, it can be avoided if an iterative approach is adopted as explained by Miles (1959)[15]. Substituting Ψ in Eq. (21) yields

$$\sigma^2 = g\kappa = gk/\sqrt{\left[1 - \left(\frac{2\Omega}{\sigma}\right)^2\right]} \tag{26}$$

For $m \neq 0$ and real x, eliminating λ between Eq. (25) and Eq. (26) leads to:

$$\lambda_1 \equiv \pm\sqrt{\frac{1}{2}\left(1 + \sqrt{1 + \left(\frac{x}{b}\right)^2}\right)} = \frac{J_{|m|-1}(x) + J_{|m|+1}(x)}{J_{|m|-1}(x) - J_{|m|+1}(x)} \equiv \lambda_2 \tag{27}$$

where $b = \frac{2\Omega^2 R}{g}$. The roots $x = k_n R$ of Eq. (27) are determined by the intersections of λ_1 and λ_2, which can be found numerically, leading to the natural frequencies σ_n. It will be shown in the subsequent numerical analysis that these natural frequencies can be quite different from the ones determined for the non-rotating liquid (Section II B 1). Note also that the frequencies calculated in this section are for an observer in the rotating reference frame, whereas the frequencies in Section II B 1 are for an observer in a fixed reference frame.

2. Solution for forced oscillations

In this paper, we consider primarily forced oscillations of the free surface resulting from a simple harmonic translation ($cos(\sigma t)$) of the tank in a fixed, horizontal direction. The mathematical formulation of this problem will be expressed for the case with liquid rotation, and a similar formulation for the non-rotating case can be obtained by assuming $\Omega = 0$. Measuring θ in the rotating coordinate system such that the angle between the axis $\theta = 0$ and the axis of translation is Ωt, the resulting boundary condition is

$$u|_{r=R} = U cos(\sigma t)\, cos(\theta + \Omega t) = \frac{1}{2} U \Re(\epsilon^+(\theta, t) + \epsilon^-(\theta, t)) \tag{28}$$

$$\epsilon^{\pm}(\theta, t) = \exp\{i[(\sigma \pm \Omega)t \pm \theta]\} \tag{29}$$

where U is the amplitude velocity of the tank oscillation. The solution of Eq. (20) satisfying the above boundary condition is found by Miles (1959)[15] and reads as:

$$\psi = \frac{1}{2} U \Re(\psi^+(r, z)\epsilon^+(\theta, t) + \psi^-(r, z)\epsilon^-(\theta, t)) \tag{30}$$

$$\psi^{\pm}(r,z) = -i(\sigma \mp \Omega)\left\{ r - \sum_n \frac{A_n^{\pm} J_1(k_n r)\cosh[\kappa_n(z+h)]}{\cosh[\kappa_n h] - (\sigma \pm \Omega)^{-2}\kappa_n g \sinh[\kappa_n h]} \right\} \tag{31}$$

$$A_n^{\pm} = \frac{2R(\sigma \pm \Omega)(\sigma \pm 3\Omega)}{\left[(\sigma \pm \Omega)^2 (k_n R)^2 - (\sigma \mp \Omega)(\sigma \pm 3\Omega)\right] J_1(k_n R)} \tag{32}$$

where the k_n are determined by Eq. (25), and $\kappa_n = k_n / \sqrt{\left[1 - \left(\frac{2\Omega}{\sigma}\right)^2\right]}$. This solution can be used to evaluate the free surface displacement, which now becomes:

$$\xi = \frac{U}{2g} \Re(\psi^+(r,z)\epsilon^+(\theta,t) + \psi^-(r,z)\epsilon^-(\theta,t)) \tag{33}$$

The horizontal hydrodynamic force on the tank can be calculated by integrating $\rho\psi$ over the vertical walls of the cylinder. This integration in the fixed reference frame yields:

$$F_x = \frac{\pi U R \rho}{2} \Re(F^+\epsilon^+(-\Omega t, t) + F^-\epsilon^-(-\Omega t, t)) \tag{34}$$

$$F_y = \frac{\pi U R \rho}{2} \Re(F^+\epsilon^+(-\frac{\pi}{2} - \Omega t, t) + F^-\epsilon^-(-\frac{\pi}{2} - \Omega t, t)) \tag{35}$$

where

$$F^{\pm} = -i(\sigma \mp \Omega)\left\{ Rh - \sum_n \frac{A_n^{\pm} J_1(k_n R)\sinh[\kappa_n h]/\kappa_n}{\cosh[\kappa_n h] - (\sigma \pm \Omega)^{-2}\kappa_n g \sinh[\kappa_n h]} \right\} \tag{36}$$

and it is assumed that at $t = 0, \theta = 0$ and $\theta = -\frac{\pi}{2}$ correspond to the x and y axes, respectively .

III. LABORATORY EXPERIMENTS

A. Experimental set-up

Forced-motion sloshing experiments with a scaled model of a closed rigid cage for salmon farming (Figure 2) were performed at the CNR-INM Sloshing Lab in Rome. The model was made of plexiglass in the shape of a right circular cylinder with internal and external diameters of 940 mm and 980 mm, respectively. It was filled with water to a level of 470 mm, measured from the bottom. A six-degree-of-freedom mechanical rig (Mistral by Symetrie), consisting of a hexapod and a rigid platform on the top, was specifically designed for sloshing experiments at the CNR-INM. The model tank was firmly mounted on the rig top platform through an in-house designed multicomponent aluminium balance which uses piezo-electric force transducers (Kistler 9366CC). The purpose of the latter was to measure the forces and

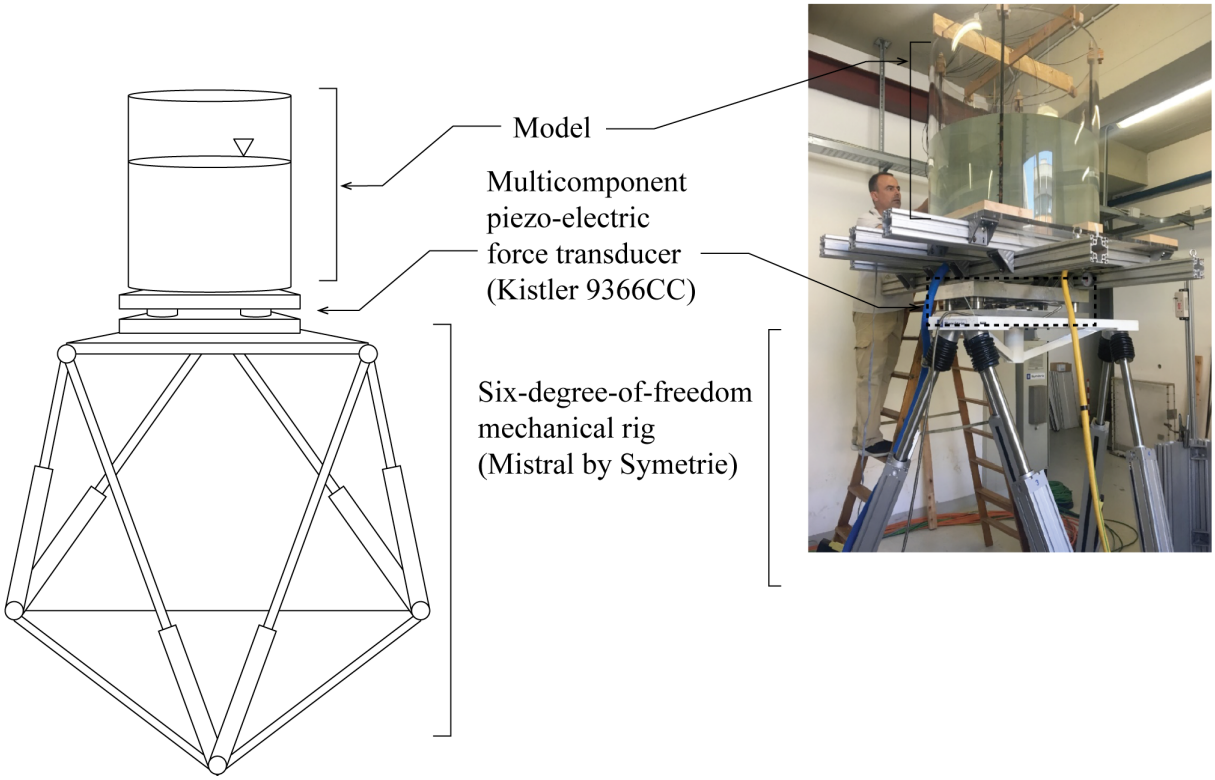

FIG. 2. Experimental set-up.

moments induced by sloshing in the tank. The main characteristics of this load-measurement system are given by Antuono and Lugni (2018)[26]: the piezo-electric technology ensured the measurement without any displacement of the sensors; the structural natural frequency (of the rig) was around 600 Hz; the system was calibrated and certified by Kistler to a maximum linearity error less than $0.1\%FSO$ (Full Scale Output) and a cross-talk error less than 1%; FSO was certified along each measurement axis, for a value of $FSO = 0.3$ kN. The acquisition of data from these sensors was set to a sampling rate of 10000 Hz.

In all experiments, the tank was undergoing sinusoidal lateral motions $x(t)$ with a constant frequency $f = 1/T$. In order to reduce the transient regime related to the dependence on the initial conditions, a ramp function on the motion amplitude has been prescribed for the first N oscillations, according to the following law:

$$x = A(t)\sin\left(2\pi\frac{t}{T}\right)$$

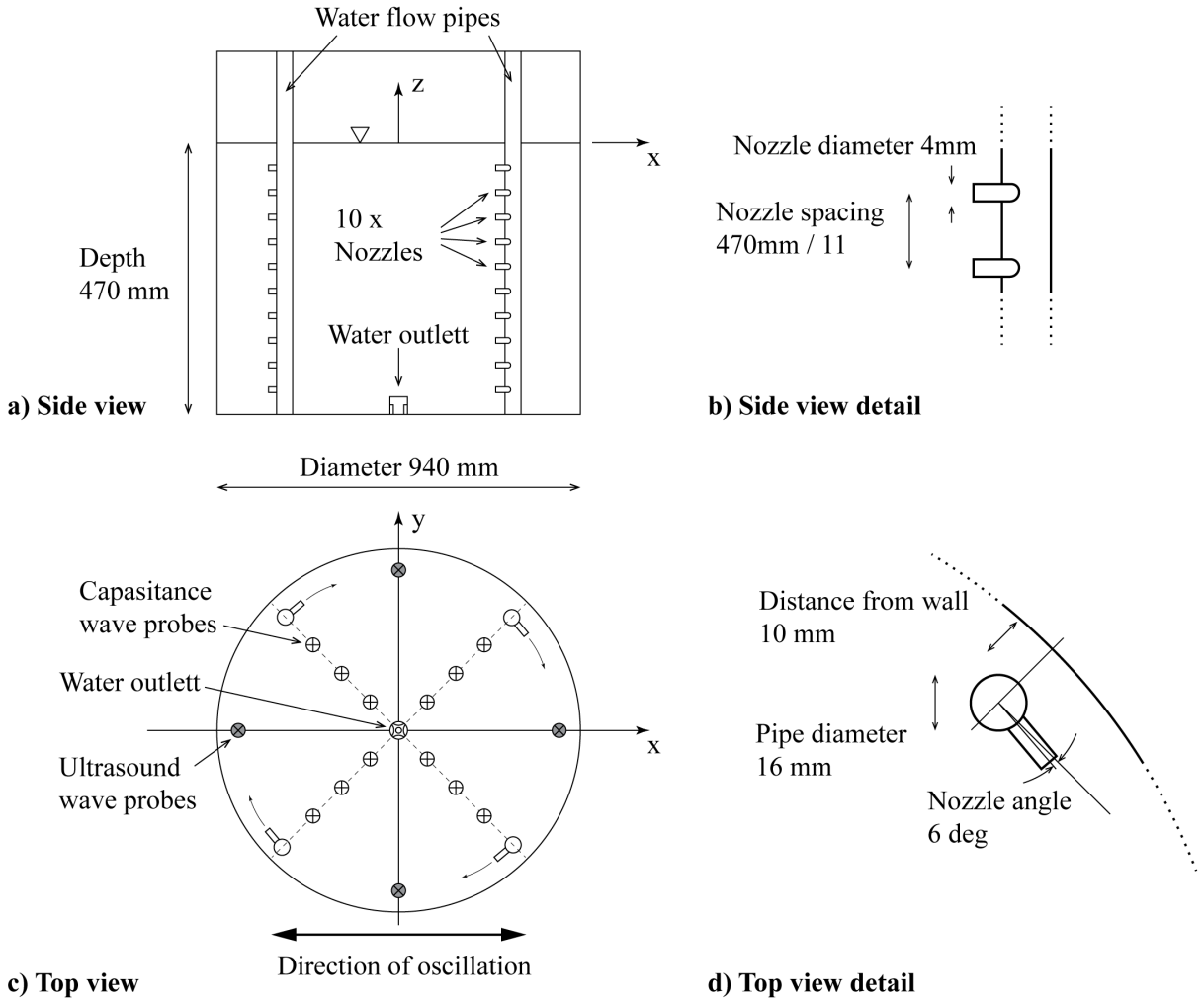

FIG. 3. Sketch of the nozzle configuration (a, b, d) and of the wave probes arrangement (c).

with $A(t)$ the amplitude varying in time according to the following function:

$$A(t) = \begin{cases} \frac{1}{2}A_0(1 - \cos(2\pi\frac{t}{T_r})) & \text{if } 0 \leq t \leq T_r \\ A_0 & \text{if } t > T_r \end{cases}$$

where the time duration of the ramp function, $T_r = NT$, is proportional to the forcing period. In our experiments $N = 20$ has been chosen for the planar wave cases, while $N = 40$ for the swirling wave cases. This initial ramp contributes to reduce the transient effects on the wave evolution inside the tank. A specific study about the transient effects and the possible hysteretic behavior characterizing the sloshing flow in the cylindrical tank is of interest and will be the focus of future investigations. Various excitation amplitudes A_0 and frequencies f were used as presented in the subsequent sections. A specific wire

potentiometer and an encoder are used to measure the time history of the imposed motion and the hexapod velocity. Two accelerometers, on the balance and on the top of the tank, respectively, are used; they enable the force measurement to be depurated by the inertial forces induced by the tank structure, In some of the experiments, tiny capacitance probes were used to measure free surface elevations at several locations across the tank (see their position in Figure 3. However, they were later removed for practical reasons in the experiments with circulating water; four ultrasound probes are mounted on the top of the tank in the position reported in Figure 3. They were collected in the latter experiments along with the force measurements and the video recordings.

B. Water-circulation system

The hydraulic system with 4 vertical pipes inside the cage shown in Figure 3 was designed to circulate water inside the cage by generating a steady rotating flow. Each of the pipes had 10 evenly distributed inlets – nozzles with a diameter 3 mm (Figure 4) – directing the water nearly tangentially to the tank walls. An external pump with large flow rate was supplying water to this hydraulic system, while a valve and a pressure gauge allowed controlling the flow rate. An outlet was placed in the bottom of the tank, in its centre, discharging the water back to the pump.

The hydraulic system was calibrated to set the water volume inside the tank in rotation at a given rotation rate Ω, which was approximately measured by tracking light particles on the free surface with a stopwatch. Although the flow was not strictly uniform, the assumption of a rigid-body rotation (see Section II A) was fair for the largest part of the tank's internal domain, except for a relatively narrow column of water in the central region, where a vortex system was formed, supported also by the outflow in the center of the tank bottom. To reduce this effect, potentially dangerous for the generation of ventilation on the pump, a suitably designed plastic cover has been used on the tank central hole.

C. Considerations on scale and viscous effects

The conducted model tests were designed to be relevant for generic closed fish cages

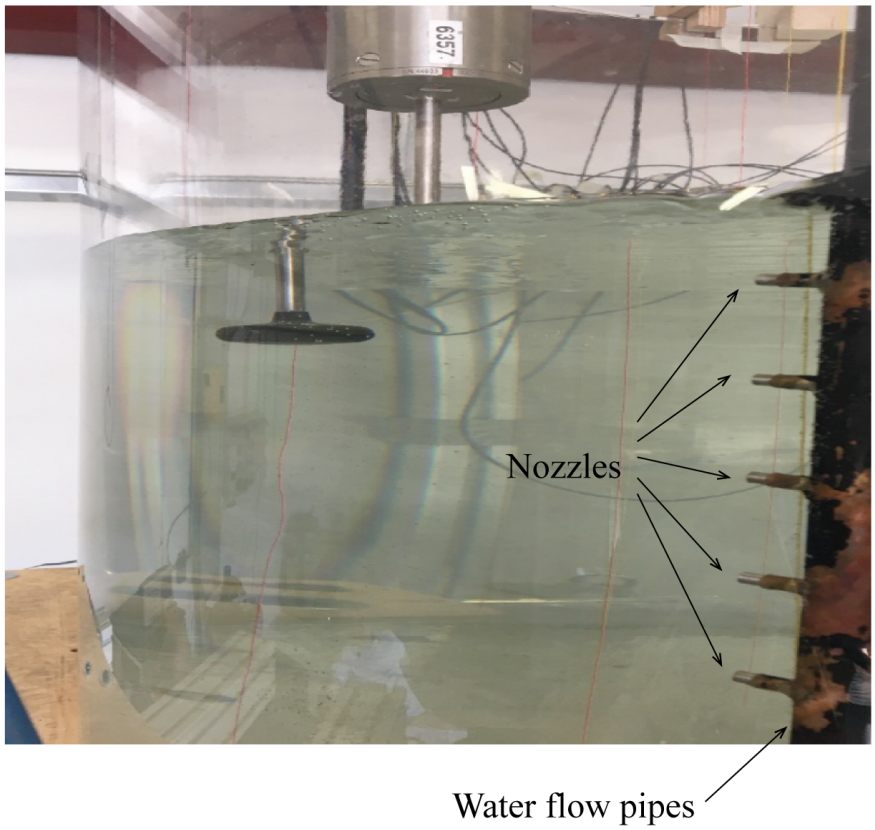

FIG. 4. Nozzles generating water flow in the tank.

for salmon aquaculture with typical full-scale containment diameter in the range 20 m to 60 m. Hence, relevant scale factors are in the range 20 to 60. Geometric scaling applies for the model geometry, while Froude scaling applies for the surge excitation frequency of the model ($\omega = \omega_{FS}\sqrt{(R/r)}$) as well as the angular velocity of the rotating water body ($\Omega = \Omega_{FS}\sqrt{(R/r)}$), with ω_{FS} and Ω_{FS} the corresponding quantities in full scale, and R the radius of the full scale prototype. There are several viscous effects in the model tests that might represent a scaling issue. The pipes used for the water circulation system (see Fig. 3) appear as vertical circular cylinders inside the tank that experience drag forces due to the rotating body of water. Correspondingly, the body of water experience counter forces from the pipes. The Reynolds number for the cross-flow of the pipes due to the steady circulation of water can be written $R_n = r\Omega d/\nu$, where for a given pipe, r is the radial position in the tank of the pipe axis from the tank axis, d is the external diameter of the pipe, Ω is the angular velocity of the body of water and ν is the kinematic viscosity coefficient. In the model experiments for the largest rotation speed $\Omega = 0.55$ rad/s, the Reynolds number

was $R_n = 4000$, i.e. sub-critical flow regime, which means laminar flow near the pipe with a turbulent wake in the far field ($Rn > 200$). The corresponding Reynolds number in full scale based on Froude scaling with scale factor $\lambda = 20$ is $R_n = 2 \times 10^5$, around the critical Reynolds number for a smooth circular cylinder. The change of drag force on the pipes due to transition from laminar to turbulent boundary layer flow will influence the required discharge of momentum from the nozzles to obtain the sought circulation speed of the water body. However, as the angular velocity of the water body is used as a test parameter, and not the discharge rate from the nozzles, this possible scaling issue is avoided.

Furthermore, during sloshing experiments with internal flow, the flow velocity can be decomposed into a mean velocity component U_0 and an oscillatory velocity component with amplitude U_a. If the ratio of the oscillatory flow velocity amplitude and the mean flow velocity $U_a/U_0 > 1$ at a given location, the flow changes direction. If this occurs at the location of the vertical pipes, the induced cross-flow drag is characterized by the Keulegan-Carpenter number $KC = (U_a T)/2r$, with T the oscillation period. The KC number is depth dependent, as the flow velocity amplitude due to sloshing decays with depth. According to Faltinsen and Timokha (2009)[24], if $KC < 10$, the depth dependent drag coefficient can be approximated as $C_D(z) = C_1 KC(z)$ where the constant $C_1 \approx 0.2$ for sub-critical flow. The associated drag force causes dissipation of energy and hence represent a damping mechanism for sloshing. This damping is found to be small in the model tests. In full scale, turbulent flow separation will likely cause reduced drag coefficient and hence reduced damping effect on sloshing. For these reasons, to properly evaluate the effects of the internal current, we have repeated the tests and compared the results with and without internal currents.

IV. RESULTS AND DISCUSSIONS

A. Various sloshing regimes

Depending on the forcing frequency, f, various sloshing regimes were observed in the experiments. These regimes are characterized by different shapes and amplitudes of the wave patterns on the free surface of the liquid. Possible wave patterns at excitation frequencies close to the lowest natural frequency ($f_1 = \sigma_{1,1}/2\pi$) are shown in Figure 5, and some examples of other sloshing regimes at higher frequencies are shown in Figure 6. Following

the multimodal sloshing theory (Section II B), these wave patterns can be considered as various superpositions of excited natural modes. According to linear sloshing theory, only natural modes with the azimuthal number equal to 1 can be excited in a rigid circular cylinder[24]. However, other sloshing modes may also be excited due to various nonlinear effects, as can be clearly seen, e.g., in Figure 5c) and Figure 6a). The most pronounced nonlinear effects, which may cause high wave responses, are mainly observed at excitation frequencies close to f_1.

Royon-Lebeaud et al. (2007)[11] studied three substantially different regimes in the non-rotating liquid: planar waves, swirling waves and chaotic sloshing (as shown in Figure 5), which can be observed when the forcing frequency f is close to the lowest natural frequency f_1. They showed that when $f < f_1$, chaotic sloshing and wave breaking may occur quasi-periodically in the following order: growth of planar wave amplitude at a rate depending on the forcing amplitude, collapse, irregular swirl and again growth of planar wave amplitude. When the forcing frequency is slightly larger than f_1, planar wave motion may bifurcate to a swirling wave regime, the amplitude of which grows exponentially and saturates at a certain value. As the amplitude of the swirling wave is significantly larger than the planar-wave amplitude (compare Figure 5b) and c)) at the same excitation parameters, the coexistence of these regimes may represent a critical design consideration for floating closed cages.

In the presence of rotation, the resonant sloshing regimes near f_1 were altered, however, the wave patterns were qualitatively similar to those in the non-rotating liquid (Figure 5). We study both the amplitude- and force responses at these sloshing regimes in more detail in the subsequent sections.

B. Free surface displacement

In this section we briefly analyse the free surface displacements obtained from the wave probes in the experiments without rotation. As these data showed good correlation with the corresponding measurements of the horizontal force on the tank, the latter were used to characterise sloshing regimes in the experiments with a rotating liquid.

In the experiment without rotation, wave amplitudes due to sloshing were accurately measured with the capacitance probes placed at multiple positions in the tank (Figure 3). The outermost probes were located at 20 mm from the tank wall along and perpendicular to

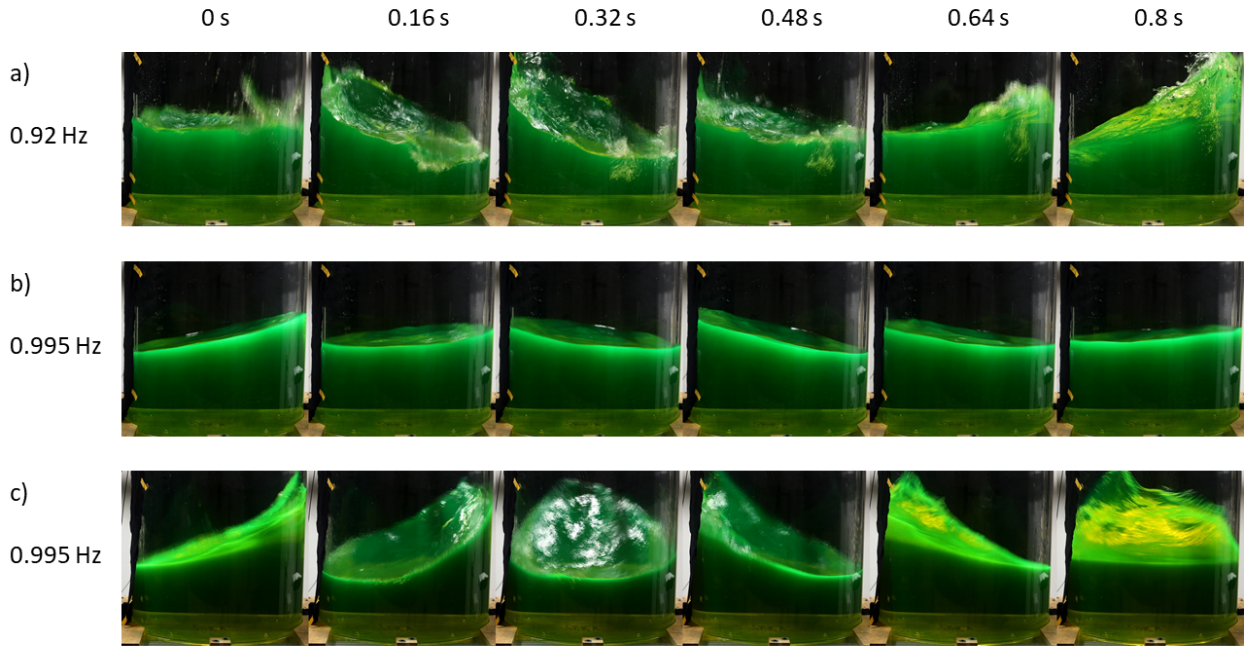

FIG. 5. Irregular (a), planar (b) and swirling (c) wave regimes observed in the sloshing experiments with a non-rotating liquid at excitation frequencies close the lowest natural frequency and excitation amplitude 5 mm. The time between two successive images is 0.16 s.

the direction of forced motion and thus allowed measuring nearly maximum wave amplitudes in both directions. These wave amplitudes, b, obtained at steady states are plotted in Figure 7 against the nondimensional excitation frequency f/f_1. The different marker shapes correspond to the three different forcing amplitudes ($A/R = 0.006, 0.011, 0.032$, where R is the tank radius); the empty markers correspond to planar waves, and the full ones indicate swirling. The experimental results shown with the black markers are compared with different numerical solutions: one, obtained with WAMIT according to linear potential theory, the second solution is predicted by the nonlinear modal approach (Section II B), and the third solution is predicted by the simplified linear theory ($n = 1$) presented in Section II C . As can be seen, all the models can accurately predict the amplitudes of the planar waves. However, the difference between these models becomes significant at excitation frequencies close to a natural frequency. Firstly, linear theory predicts typical resonance curves with infinite wave amplitudes, as the wave motion is undamped, and secondly, the swirling regime at $f \approx f_1$ is not captured. In contrast, the nonlinear model predicts the occurrence of swirling waves

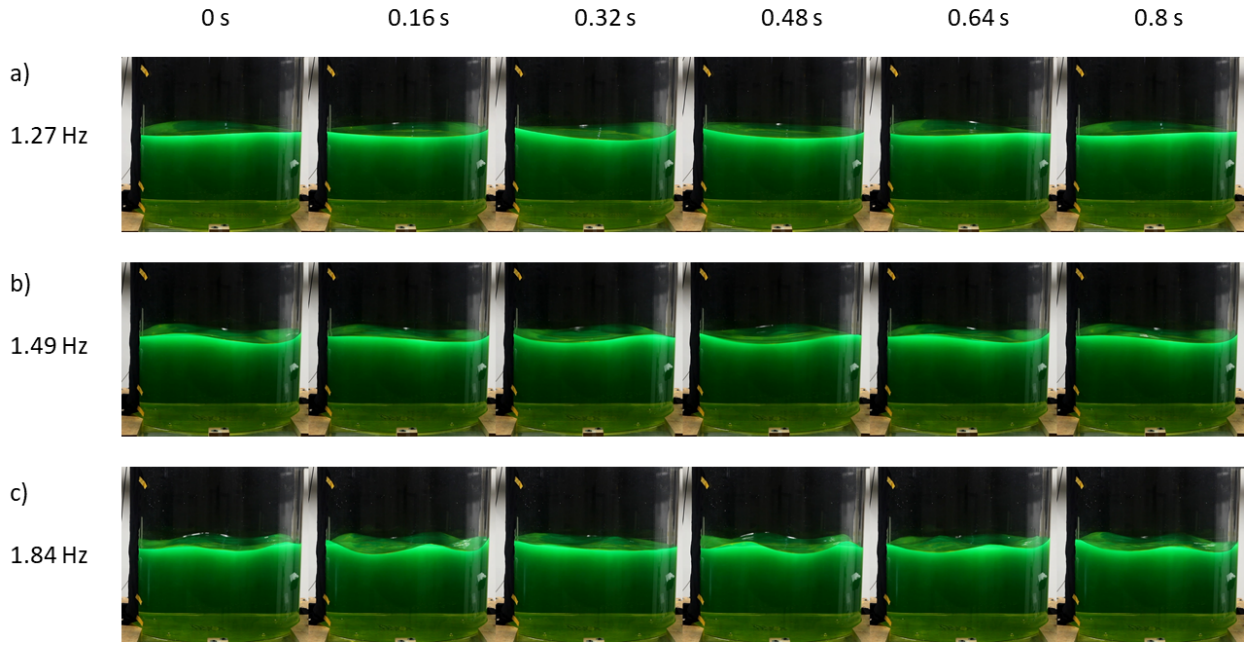

FIG. 6. Various wave patterns observed in the sloshing experiments with a non-rotating liquid at different excitation frequencies (given under a, b and c) and excitation amplitude 5 mm. The time between two successive images is 0.16 s.

near f_1, and their amplitudes seem to compare well with the experimental points.

As only two points (at $f \approx f_1$) corresponding to swirling were obtained in these experiments, the numerical simulations with the nonlinear model were extended to slightly higher frequencies to demonstrate that the swirling- and planar-wave regimes may coexist. In this model, a steady-state swirling wave was fist established at $f \approx f_1$ and then the excitation frequency was gradually increased, leading to new steady-state swirling regimes with larger wave amplitudes. Increasing the excitation frequency too fast would instead lead to a planar regime with a much smaller wave amplitude, as shown in Figure 7, at $f/f_1 \approx 1.1$. Thus, both regimes are possible for a wide range of excitation frequencies. As swirling waves are characterised by much greater wave amplitudes than their planar counterparts, and great internal waves usually imply great loads, the swirling wave regimes are of particular concern for the design of floating closed cages. We discuss sloshing-induced loads in the next section.

The nonlinear model predicted also irregular waves (with unsteady amplitudes) at a range of excitation frequencies slightly lower than f_1, which was also observed in the experiments

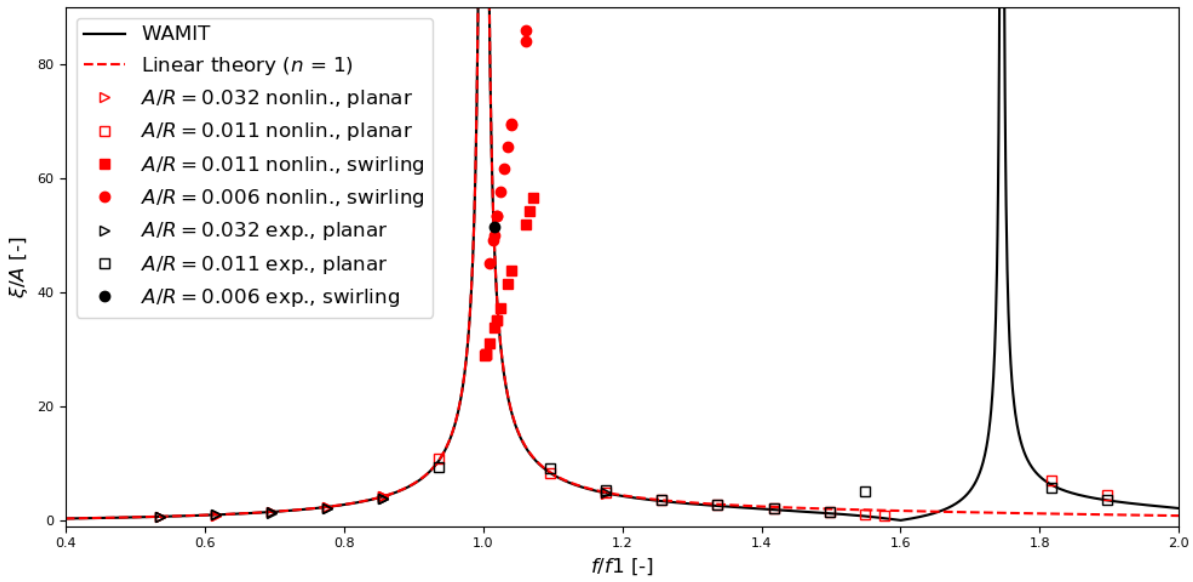

FIG. 7. Experimental and numerical maximum steady-state wave elevations, normalised with the displacement amplitude A, for different forcing frequencies and amplitudes. Empty markers correspond to planar regimes, and filled markers imply swirling. All data are for the non-rotating liquid sloshing in the tank with the circulation system removed.

(e.g., Figure 5 a). These waves represent a transition between a planar regime and swirling, and thus may reach the same amplitude as the swirling wave, as already well assessed in literature, through experimental[11] and theoretical[12] studies. However, irregular waves cannot be characterised by a steady-state amplitude and therefore are not shown in Figure 7. In the experiments, similar wave regimes were also observed at excitation frequencies close to $f_{1,2}$, but their largest amplitudes were approximately in the same range as the planar waves. For these cases, WAMIT predicted an infinite resonance peak (at $f/f_1 \approx 1.75$ in Figure 7), whereas the nonlinear model predicted damped steady-state responses. Neither of these solutions agree with the experiment.

In our nonlinear multimodal analysis, the number of radial modes I_r was set to 2, which was sufficient to match both the experimental results and the WAMIT predictions outside the resonance frequencies; however, larger I_r may be needed to achieve agreement with WAMIT at high frequencies. As demonstrated, the main advantage of the employed nonlinear model, compared to the linear one, is the capability of the former to predict the nonlinear sloshing effects at excitation frequencies close to f_1 (although, only for the non-rotating liquid). From

the experiments, it was found that other nonlinear effects are possible at higher frequencies, e.g., the excitation of mode (3,1) at $f \approx f_{3,1}$ ($f/f_1 \approx 1.55$ in Figure 7) and the occurrence of irregular waves at $f \approx f_{1,2}$. Although neither method can predict these effects, they do not seem to lead to large wave motions, as compared to swirling waves at $f \approx f_1$.

C. Hydrodynamic force on the tank with a non-rotating liquid

The sloshing force on the tank parallel to the forced motion direction (F) can be identified from the measurements as $F = F_{measured} - Ma$, where $F_{measured}$ is the measured force between the rig and the tank, which is the force needed to move the tank along the given axis with the prescribed acceleration a, and M is the total mass of the cage, including the mass of the liquid. As the tank acceleration in the perpendicular direction is zero, the transverse force ($F^{\perp}$) follows directly from the measurements. Similarly, F and $F^{\perp}$ can be also obtained from Eqs. (16) – (17) and Eqs. (34) – (36) by leaving out the inertial terms. Further, F and $F^{\perp}$ are made dimensionless by dividing them by ma, where m is the mass of the contained liquid.

In the case of the non-rotating liquid, the measured forces agree well with the ones predicted by the nonlinear modal method (Section II B) for various forcing amplitudes and a wide range of frequencies, as shown in Figure 8. Moreover, the experimental points collapse on the curve predicted by the linear theory (Section II C) with $\Omega = 0$ outside the resonance. At $f \approx f_1$, the resonant swirling phenomenon may occur, as discussed in the previous section. In this case, only the predictions by the nonlinear modal method are comparable with the experimental results. Note that the transverse force $F^{\perp}$ is not plotted in Figure 8 as it is nonzero only when the swirling phenomenon occurs, and then $F^{\perp} \approx F$. The agreement between the nonresonant forces from the experiment and the predictions by the linear theory with n = 1 (equivalent to the number of radial modes in the multimodal theory) suggests that high-order sloshing modes do not have a significant effect on the sloshing force, except for the regimes with swirl waves at $f \approx f_1$. Although free surface elevations may be under predicted by the linear theory with $n = 1$, as e.g., at $f/f_1 \approx 1.55$ in Figure 7, the corresponding prediction of the sloshing force agrees with the experiment within the measurement accuracy (see Figure 8). Thus, we may use n = 1 in all our linear analyses, in which resonant phenomena other than that at $f \approx f_1$ are outside the scope of this study.

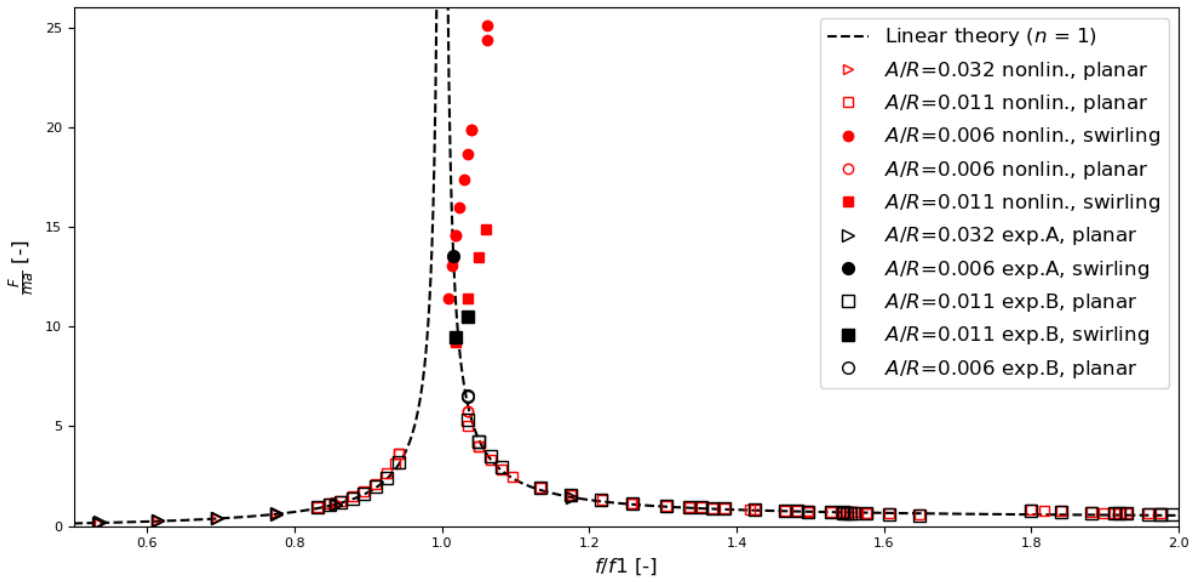

FIG. 8. Nondimensional sloshing-induced force on the tank along the excitation direction. All data are for the non-rotating liquid sloshing in the tank with the circulation system removed ($\Omega = 0$ rad/s). The markers are explained in Figure 7. The transverse force $F^{\perp}$ is not plotted, since $F^{\perp} \approx F$ at swirling regimes and 0 otherwise.

D. Hydrodynamic force on the tank with a rotating liquid

Similar to the analysis in the previous section, here we consider the longitudinal and transverse sloshing forces F and $F^{\perp}$, respectively, acting on the tank with a rotating liquid. As the nonlinear modal approach (Section II B) is not applicable for rotating liquids, the only theory we refer to here is the one presented in Section II C. Experimental data were obtained for cases with different rotation rates Ω and a fixed set of excitation frequencies between 0.86 and 1.1 Hz. In the case with $\Omega = 0.33$ rad/s, a broader range of frequencies, 0.5 – 2.0 Hz, was used to allow comparison with the non-rotating cases in Figure 8. For the same reason, all frequencies in this section are scaled with f_1, which is the lowest natural frequency of sloshing in the non-rotating liquid. Unless stated otherwise, the amplitude of the forced motion was 5 mm, i.e., $A/R \approx 0.011$.

Figure 9 shows the forces obtained from the experiments and compares them to the linear theoretical predictions for a liquid rotating at $\Omega = 0.33$ rad/s. By comparing these results with those in Figure 8, one can immediately observe that the transverse force $F^{\perp}$ is nonzero

for a much wider range of frequencies ($0.8 < f/f_1 < 1.2$) when the liquid is rotating. The cases with a nonzero $F^{\perp}$ correspond to swirling wave regimes. Unlike the case with the non-rotating liquid, the experiments with $\Omega = 0.33$ rad/s show also stable swirling waves at "nonresonant" frequencies, e.g., $f/f_1 < 0.95$ and $f/f_1 > 1.1$; however, the force amplitudes at these frequencies are significantly lower than those at $f \approx f_1$, where violent swirling waves occur. It is thus demonstrated that rotation introduces linear swirling regimes, which were not observed previously in the non-rotating liquid sloshing. From the theoretical point of view, linear swirling waves in a rotating liquid are not surprising and are the consequence of the Coriolis term in Eq. (19). In fact, both F and $F^{\perp}$ are accurately predicted by the adopted linear theory for a wide range of frequencies, except the cases at $f \approx f_1$, as shown in Figure 9.

The sloshing behaviour at $f \approx f_1$ shown in Figure 9 is nontrivial and appears to be quite different from the nonlinear sloshing of the non-rotating liquid shown in Figure 8. It is also strongly nonlinear, as the experiments with different motion amplitudes ($A/R \approx 0.011$ and $A/R \approx 0.006$) suggest, including stable and unstable regimes, which are difficult to characterise based on available theories. Therefore, the identification of steady-state force amplitudes from the experiments at $f \approx f_1$ with rotation can be challenging. In some cases, the measurements showed long-lasting beating effects and instabilities of apparent steady sloshing regimes. One example is shown in Figure 10, where the force first appears to be steady, but after 5 minutes it collapses and turns into a beating force. This example corresponds to the maximum measured force in Figure 9 (as obtained from the first 5 minutes of the measurement), whereas the other tests at greater f show lower steady-state amplitudes, which match with the linear predictions.

E. Effect of rotation on resonant sloshing

To study the effect of rotation on the resonant sloshing near the fundamental frequency f_1, several experiments were conducted at different rotation rates Ω in the range $0 - 0.55$ rad/s and a fixed motion amplitude $A/R \approx 0.011$ for a set of excitation frequencies f between 0.86 and 1.1 Hz with 0.02 Hz (or 0.01 Hz) regular increments . At these frequencies, sloshing of the non-rotating liquid may occur at three different regimes, as discussed in Section IV A: chaotic waves with unstable amplitudes at $f \lesssim 1$ and steady-state swirling or planar waves

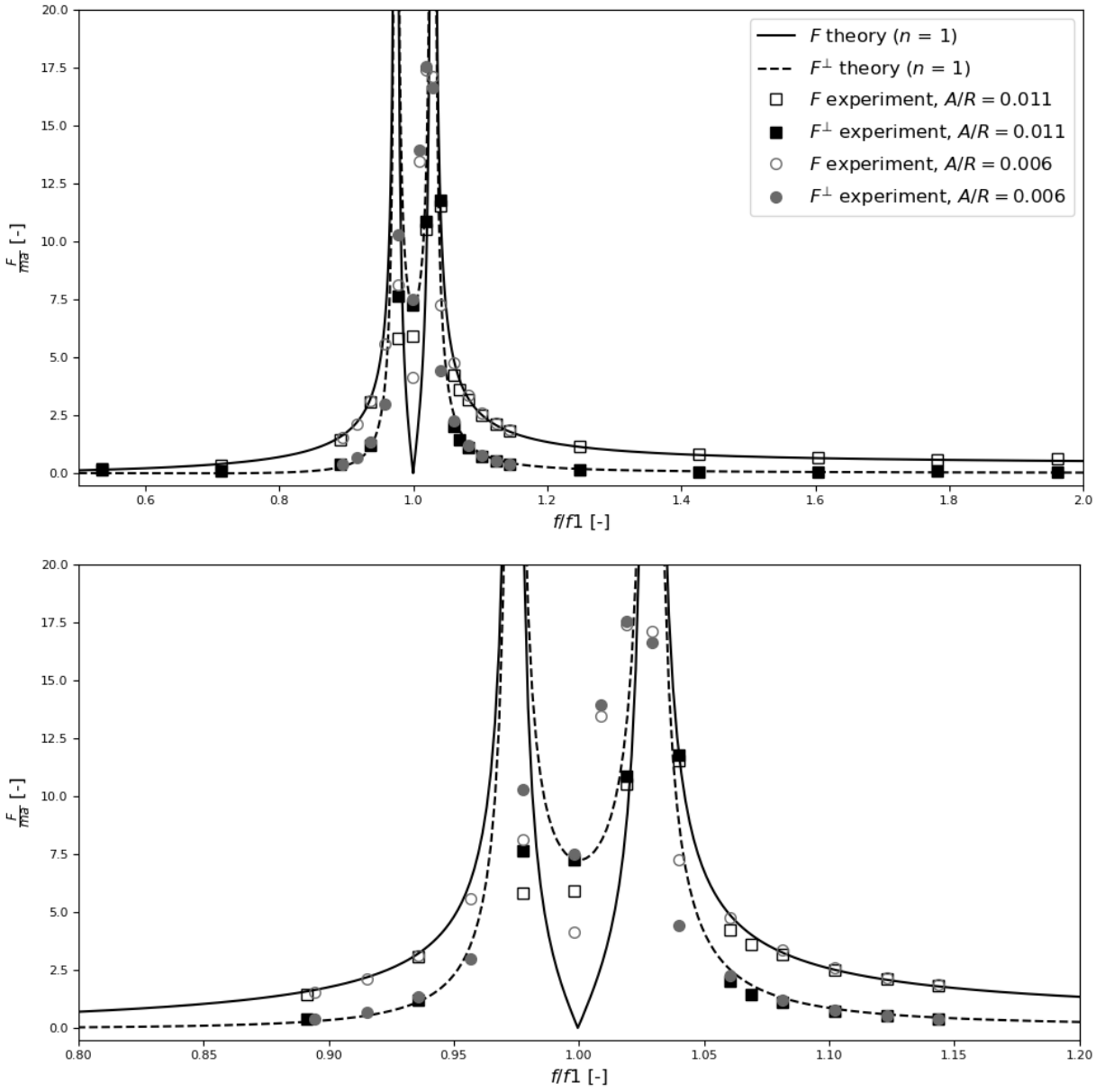

FIG. 9. Top panel: Nondimensional sloshing-induced forces on the tank with a liquid rotating at $\Omega\,(R/g)^{0.5} \approx 0.07$ ($\Omega = 0.33$ rad/s). $F^{\perp}$ is the transverse force.

Bottom Panel: Enlarged view around the first resonance frequency range

at $f \gtrsim f1$ (e.g., as shown in Figure 8). In the presence of rotation, these regimes are altered (as indicated in Figure 9) and, according to the theory, different resonance curves should be observed depending on Ω. The effect of Ω is demonstrated in Figure 11 – Figure 14, where both the theoretical resonance curves and the experimental data are presented.

The linear theory for a rotating liquid predicts a pair of resonance frequencies, $f^{-} <$

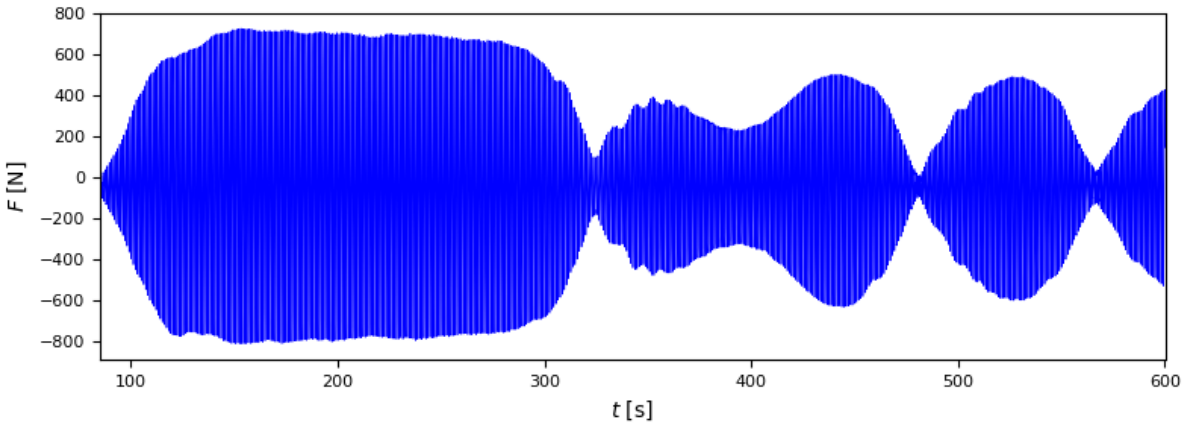

FIG. 10. Collapse of an apparent steady-state swirling force after a long time with constant $A/R = 0.006$ and $f/f_1 = 1.03$ in the experiment at $\Omega\,(R/g)^{0.5} \approx 0.07$ ($\Omega = 0.33$ rad/s).

$f_1 < f^+$, splitting the resonance curve at $f = f_1$ and leading to infinite sloshing responses at $f = f^-$ and $f = f^+$ and a finite amplitude at $f = f_1$, where $F^\perp$ is nonzero. The experimental results in terms of F and $F^\perp$ show an agreement with the linear predictions at nonresonant frequencies and indicate the presence of the pair of natural frequencies near f_1 (see, e.g., Figure 13). However, near f^- and f^+, the experimental results deviate from the theoretical predictions, indicating the occurrence of strong nonlinear effects in this frequency range. Like in the case with the non-rotating liquid at $f \lesssim f_1$, the sloshing in the rotating liquid is chaotic at $f \lesssim f^-$, and therefore there is no experimental data with a steady-state amplitude at $f/f_1 \approx 0.96$ (0.92 Hz) in, e.g., Figure 13. In fact, we observed chaos in all experiments at $f/f_1 \approx 0.96$ and $A/R \approx 0.011$ independent of Ω.

Nonlinear steady-state swirling regimes in the rotating liquid can also be observed: first at $f \gtrsim f^-$ and then at greater f until a certain frequency greater than f^+, above which the nonlinear swirling switches to the linear one with a significantly lower amplitude. However, in the experiments with $\Omega \geq 0.33$ rad/s, the amplitudes of the F and $F^\perp$ dropped at $f \approx f_1$, whereas the amplitude of the swirling wave in the non-rotating liquid should increase monotonically with f (see Figure 8). Moreover, in the former experiments, the sloshing-induced forces at $f = f_1$ were significantly lower than those in the experiment without rotation (compare Figure 11 and Figure 14). We discuss this sloshing suppression effect in Section IV H.

The direction of the swirl motion is opposite to that of the current (Ω) at $f < f_1$, but it

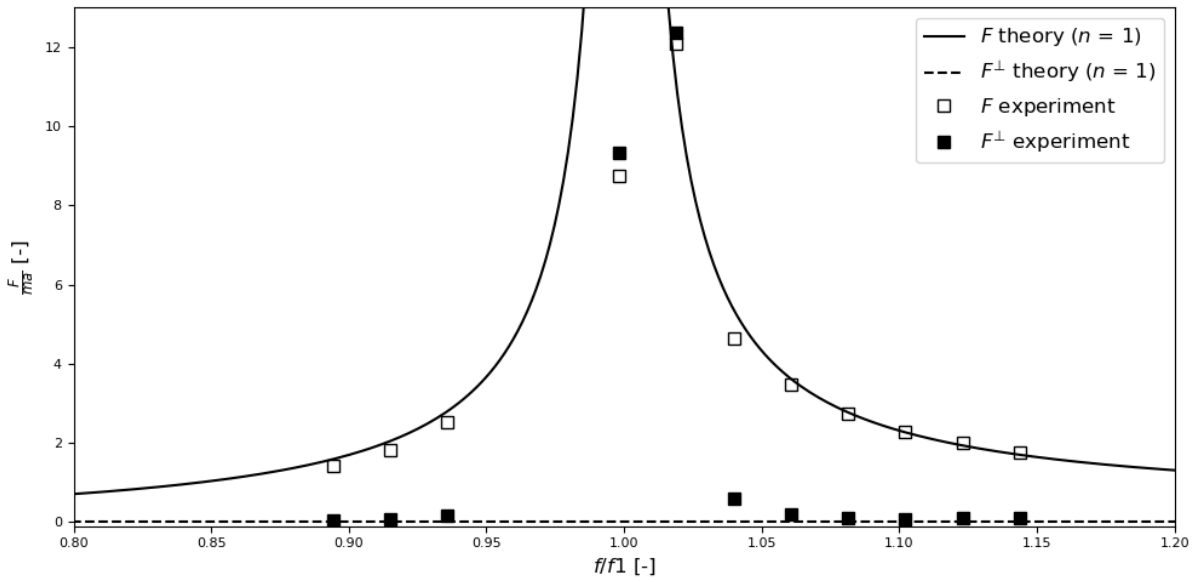

FIG. 11. Nondimensional longitudinal and transverse sloshing-induced forces on the tank with the circulation system installed but deactivated (i.e., $\Omega = 0$).

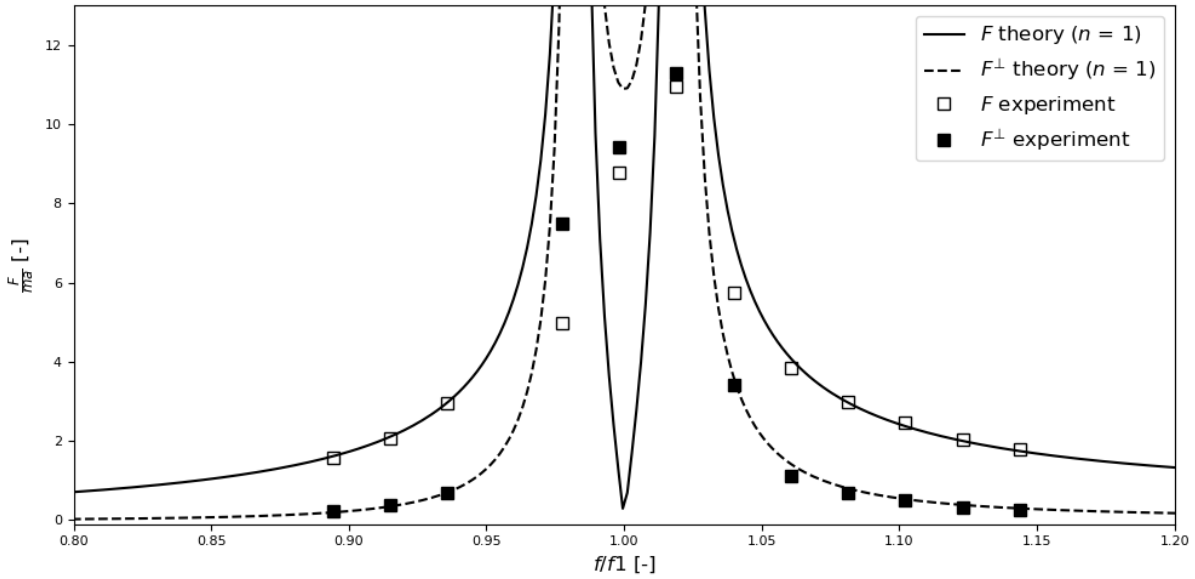

FIG. 12. Nondimensional longitudinal and transverse sloshing-induced forces on the tank with a liquid rotating at $\Omega\,(R/g)^{0.5} \approx 0.05$ ($\Omega = 0.22$ rad/s).

inverts at $f \approx f_1$ and at $f > f_1$, both the swirl and the current move in the same direction. This behaviour can also be predicted by the linear theory considering the phase difference between F and $F^{\perp}$, which changes by 180 degree at $f \approx f_1$. The latter is verified by

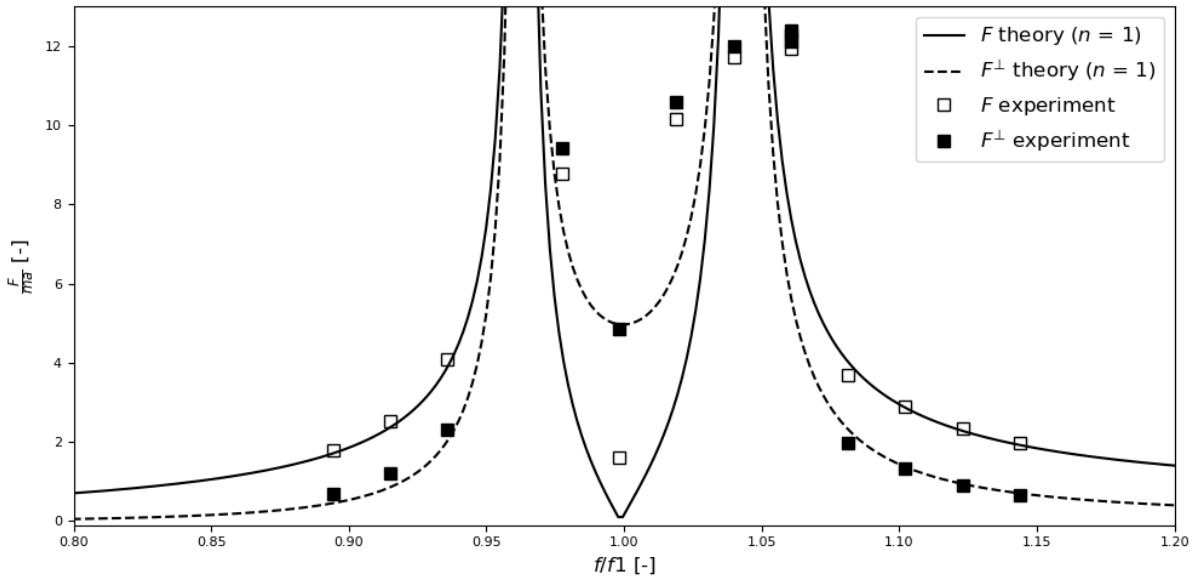

FIG. 13. Nondimensional longitudinal and transverse sloshing-induced forces on the tank with a liquid rotating at $\Omega\,(R/g)^{0.5} \approx 0.11$ ($\Omega = 0.48$ rad/s).

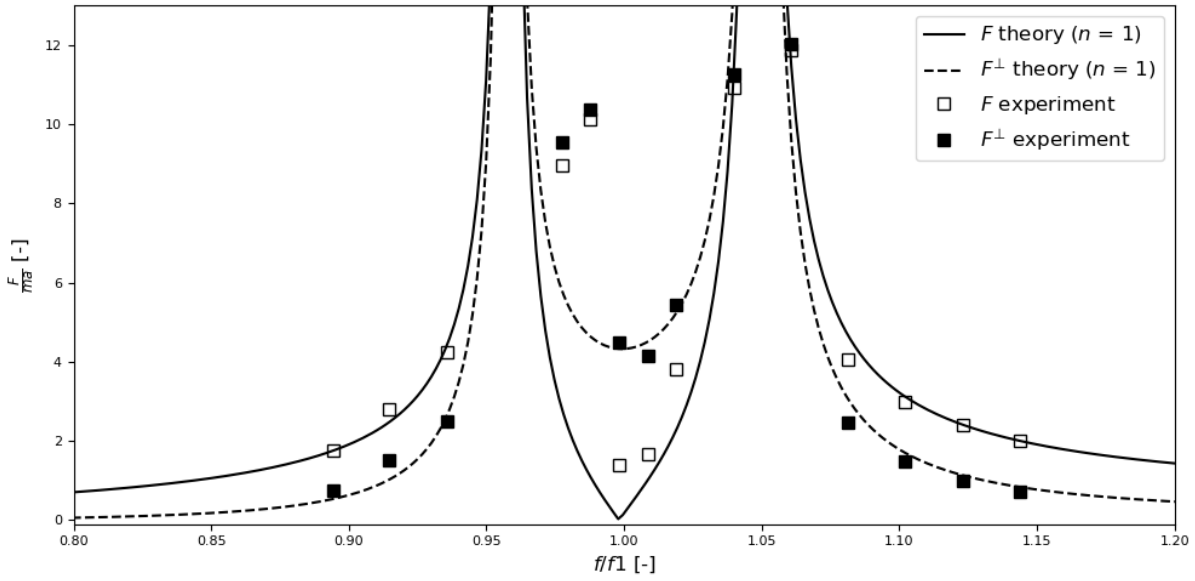

FIG. 14. Nondimensional longitudinal and transverse sloshing-induced forces on the tank with a liquid rotating at $\Omega\,(R/g)^{0.5} \approx 0.12$ ($\Omega = 0.55$ rad/s).

computing the inverse tangent of the ratio of the imaginary and real parts of the expressions in Eqs. 34 – 35 and taking the difference between them, which gives the phase difference between F and $F^{\perp}$. Both the experimental results and the theoretical predictions of the

phase appear to be nearly independent of Ω, as shown in Figure 15. The phase difference (φ) between the longitudinal force F and the cage acceleration determines the sign of the added mass coefficient associated with sloshing, whereas $\frac{F}{ma}$ (as defined in Section IV D) determines its magnitude. If $\varphi = 180°$ the added mass is positive, and if $\varphi = 0°$, it is negative.

The linear theory predicts that φ should alter from 180° to 0°, then vice versa and then again between the pair of natural frequencies f^- and f^+, which depend on Ω. A somewhat remotely similar behaviour can be observed only in the experiments at $\Omega = 0.55$ rad/s (Figure 16). However, the experiments with lower rotation rates demonstrate a different phase behaviour: φ gradually changes from 180° to approximately 90° (depending on Ω) and then abruptly drops to approximately 0°. It can also be observed that the added mass becomes negative ($\varphi \approx 0°$) earlier, i.e., at lower frequencies f, in the cases with lower Ω. This fact is important for floating aquaculture cages, for which maintaining a positive added mass for a broader range of frequencies would lead to smaller cage responses in wavy sea conditios.

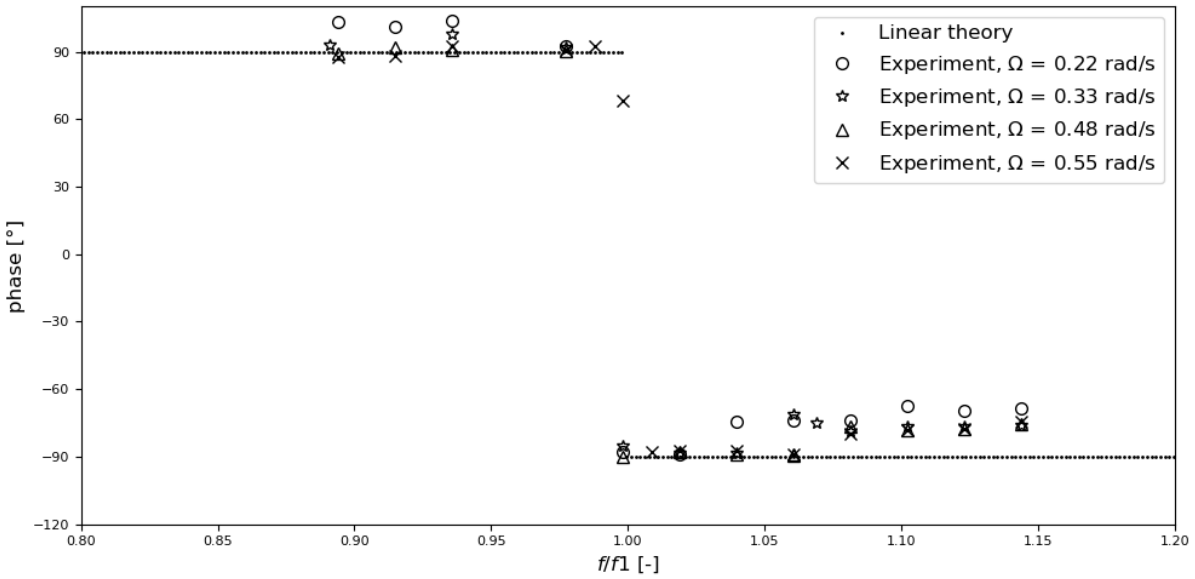

FIG. 15. Phase difference between F and $F^{\perp}$ at swirling regimes.

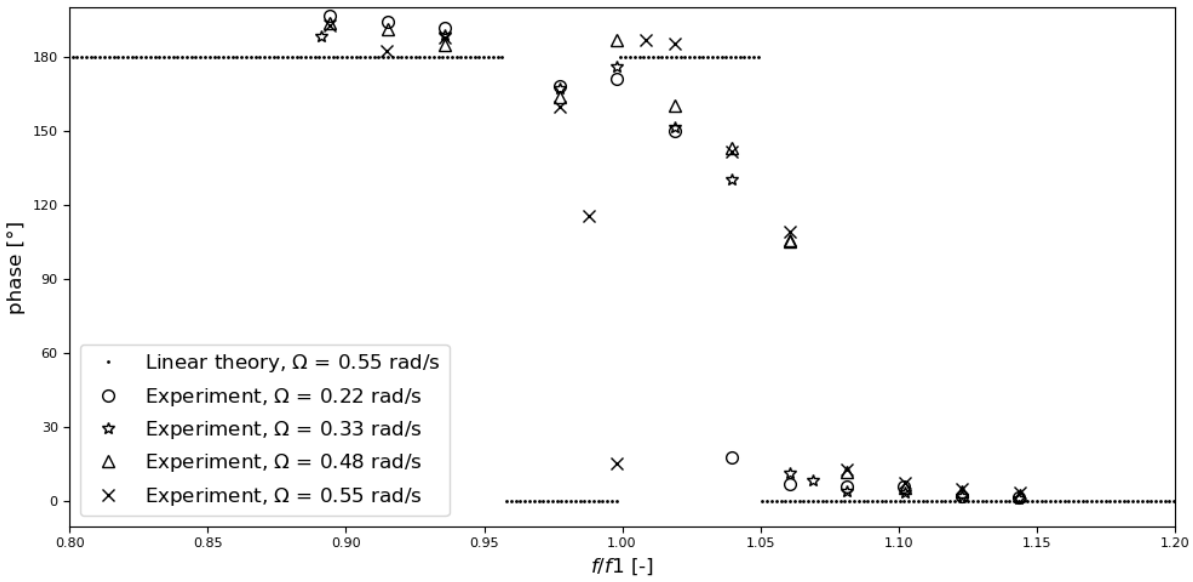

FIG. 16. Phase difference between the longitudinal sloshing force F and the acceleration of the cage.

F. Dissipation of sloshing waves

The damping ratios of the dominant sloshing mode ($\delta_{1,1}$) were evaluated from the measurements of the force (F) due to free liquid oscillations (decay tests). In these tests, the tank was instantly moved 2 or 8 cycles with an amplitude of 3 mm at frequencies near $\sigma_{1,1}$, and then the free decay of the force was measured. The force decay is assumed to be exponential in time, such that $F\ \exp(-\gamma t)$, where $\gamma = \delta\sigma$, and δ and σ have the same meaning as in Eq. (15). Thus, determining the exponential trend of the force decay leads to the identification of the damping ratio for a given natural frequency of free oscillations. However, the decay tests with the rotating liquid consistently showed two frequencies close to $\sigma_{1,1}$ causing a beating effect in the measured force (see Figure 17 and Figure 18). As will be shown later, these two frequencies are the result of the rotation-induced splitting of $\sigma_{1,1}$. It was challenging to separate these two frequencies in the decay test; therefore, we used measurements containing both harmonics and, assuming that they decay at nearly equal rates, we determined the exponential trends for successive peaks of the beating signals as shown in Figure 17 and Figure 18.

The damping ratios were evaluated for the setup with the water-circulation system at different flow rates Ω, including 0 rad/s, and for the tank with the circulation system re-

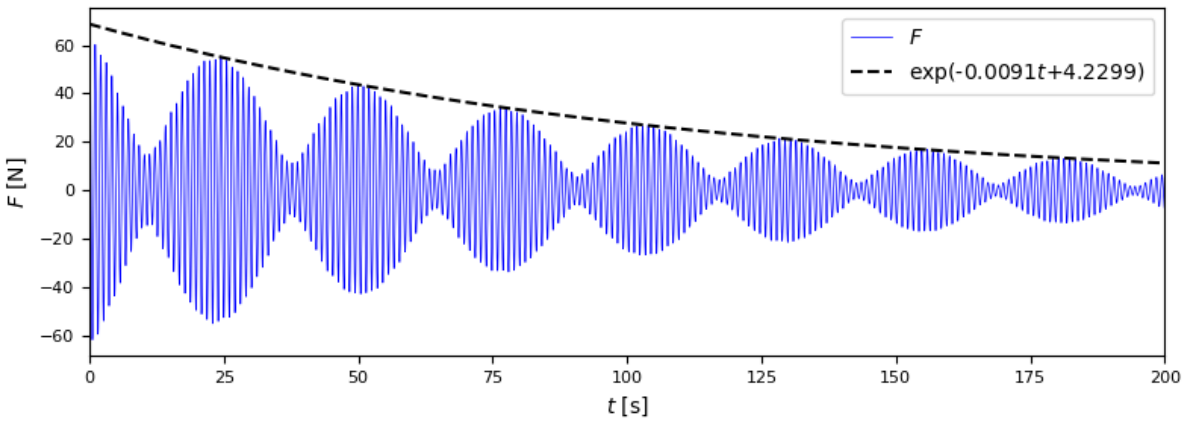

FIG. 17. . Free oscillations of the sloshing-induced force and their exponential decay trend at $\Omega = 0.22$ rad/s. The beating is caused by two dominant harmonics at approx. 0.945 Hz and 0.983 Hz, which correspond to the first pair of natural frequencies of sloshing in a liquid rotating at $\Omega = 0.22$ rad/s.

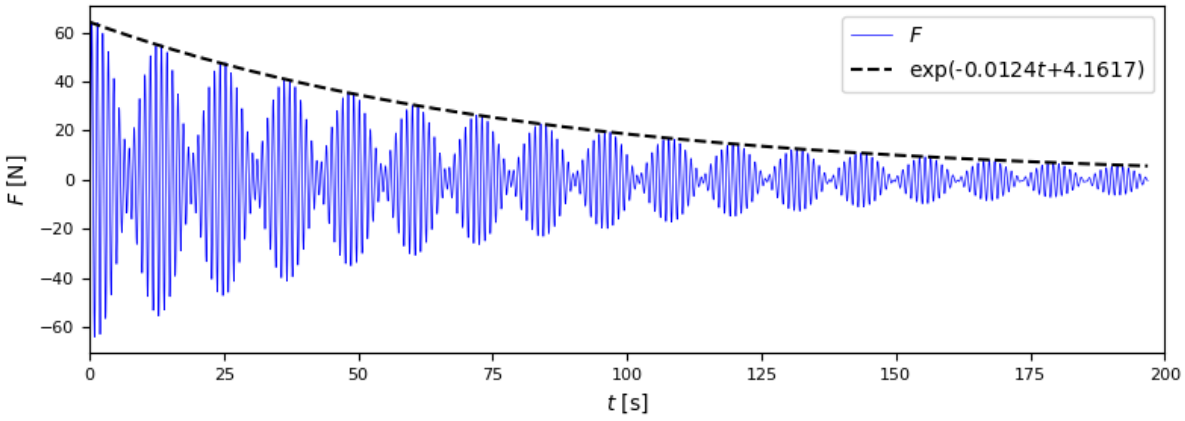

FIG. 18. Free oscillations of the sloshing-induced force and their exponential decay trend at $\Omega = 0.48$ rad/s. The beating is caused by two dominant harmonics at approx. 0.923 Hz and 1.007 Hz, which correspond to the first pair of natural frequencies of sloshing in a liquid rotating at $\Omega = 0.48$ rad/s.

moved, which is called here "bare tank". The results are summarised in Table I, which gives also an estimate for the bare tank following from Eq. (15). As can be seen, δ significantly increases with Ω and can be as much as twice greater (at $\Omega > 0.48$ rad/s) than the damping ratio for the non rotating liquid. Nevertheless, this increase of δ does not seem to lead to

any significant decrease of the sloshing force in the broad frequency range shown in Figure 9, except for a narrow band of frequencies near $\sigma_{1,1}$. However, near this resonant frequency, the effect of δ on the sloshing amplitude and phase can be significant.

Ω [rad/s]	0	0.22	0.33	0.48	0.54	Bare tank	Eq. (15)
$\delta_{1,1} \times 10^4$ [-]	11 ± 2	15 ± 2	17 ± 3	21 ± 3	22 ± 3	10 ± 2	12

TABLE I. Damping ratios for the sloshing mode with the lowest natural frequency. The experimental values are given for both the bare tank (without the circulation system) and the tank with the circulation system at different flow rates Ω.

As mentioned, the decay tests were performed by moving the tank either 2 or 8 complete cycles at a given frequency. The difference between these tests was that the latter resulted in nearly three times greater initial amplitudes of the liquid oscillations than those shown in Figure 17 and Figure 18, which both correspond to the 2-cycle excitation. The obtained measurements were used to determine whether δ could be assumed nearly independent of the initial sloshing amplitude. It was found that the damping ratios determined at lower sloshing amplitudes (2 cycles) were consistently greater than ones corresponding to greater amplitudes (8 cycles); however, the difference was less than 5%, which is nearly the same as our method accuracy (see Table I). Thus, within this accuracy, the identification of δ was not affected by the initial sloshing amplitude.

G. Rotation-induced splitting of the natural frequencies

Miles (1959) has found that one effect of rotation is to split the natural frequencies of the non-rotating liquid. Our experimental results confirm the presence of frequency pairs near $\sigma_{1,1}$ in the tank with a rotating liquid. This can be seen in both the frequency dependence of sloshing-induced forces due to forced motion (Section IV D) and free oscillations of the liquid (Section IV F). The adopted linear model has proved to be capable of predicting the exact values of the observed frequency pairs depending on the rotation rate Ω. In the further analysis, the splitting of the natural frequencies of sloshing for a range of rotation rates, $\Omega < 0.5\sigma$, is numerically evaluated for the dominant antisymmetric modes (m = 1) and the symmetric modes with m = 2 (the latter may be important for nonrigid cages). The

computational method is presented in Section II C 1 and is straightforward for a deep tank (Eq. 27). The results determined by Eq. (27) will be qualitatively similar to those for a tank with an arbitrary depth, except for cases with $h \ll 2R$[15]. Figure 19 shows the pairs of frequencies calculated for the first- and higher order modes up to $n = 3$. As seen, the effect of Ω is significant for the primary modes (n = 1) and is negligible for $n > 1$. In the absence of rotation ($\Omega = 0$), all frequency pairs converge to their counterparts for the non-rotating liquid, as defined by Eq. (3). Note that the frequencies in Figure 19 are calculated for an observer in the rotating reference frame; and in the fixed frame (as in Sections IV D – IV F for $m = 1$), they become $\sigma \mp \Omega$, where the upper and lower signs correspond to the upper and lower pairs in Figure 19, respectively. Thus, the separation between the frequencies split by rotation is in the order of Ω in the fixed reference frame and always increases with Ω.

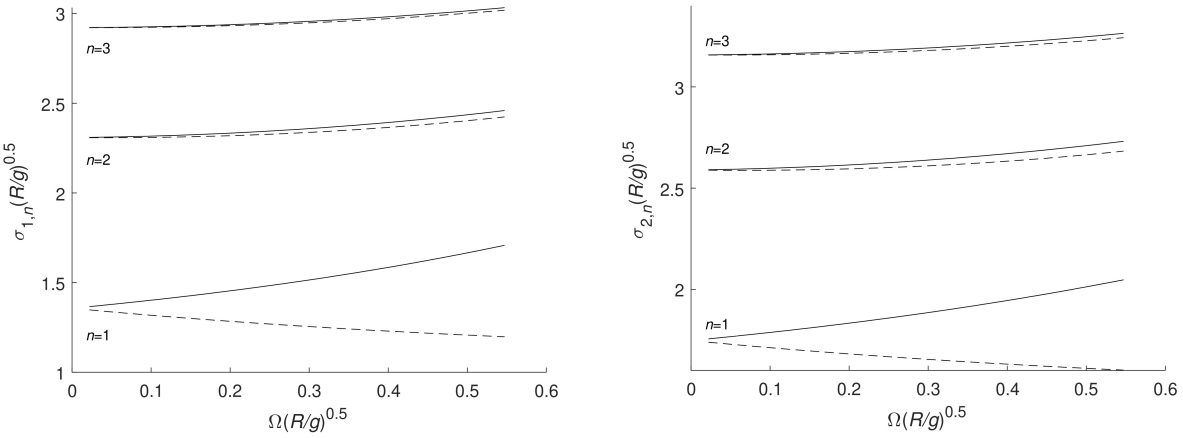

FIG. 19. Rotation-induced splitting of the first three natural frequencies of the antisymmetric slosh modes with m = 1 (left) and symmetric ones with m = 2 (right) for a deep circular tank of radius R at different rotation rates Ω. The frequencies are given for an observer in the rotating reference frame.

H. Sloshing suppression due to rotation

As shown in Section IV F, one effect of rotation is to increase the viscous damping of sloshing waves; however, this effect is not strong enough to suppress the sloshing. In contrast, the rotation-induced splitting of the natural frequencies may lead to a partial suppression of

sloshing near the natural frequency of the non-rotating liquid. The results in Section IV D indicate that at a sufficiently great separation between the pair frequencies (i.e., at great Ω), the sloshing at a resonant frequency of the non-rotating liquid may become "non-resonant", as at f_1 in Figure 13 and Figure 14. In these cases, the sloshing amplitude can be several times smaller than it would be otherwise at f_1 in the absence of rotation. Empirically, we have shown that a significant suppression effect can be observed already at $\Omega\left(R/g\right)^{0.5} \gtrsim 0.11$ and $A/R \approx 0.011$, or $\Omega \gtrsim 0.48$ rad/s and $A = 5$ mm in the model scale (see Figure 13 and Figure 14). However, in our cases, the amplitudes decreased only within a relatively narrow range of frequencies near f_1, and outside this range, new resonance peaks were observed near the altered natural frequencies. In the experiments by Saito and Sawada (2018)[16] with a much greater rotation rate $\Omega\left(R/g\right)^{0.5} \approx 0.45$ and $A/R \approx 0.02$, the sloshing was efficiently suppressed within a broad frequency range between approximately $(1 \pm 0.1) f_1$. All these results suggest that rotation may help preventing violent sloshing waves at certain frequencies of forced motion. Theoretically, sloshing due to forced motion of a closed cage can be suppressed (or made non-resonant) by altering the natural frequencies with a sufficiently great Ω. This would be possible if the frequency spectrum of the excitation forces were narrow compared to Ω, i.e., all excitation frequencies would be located between the pair of the natural frequencies altered due to rotation. However, great Ω would imply great liquid velocities in the cage, which may not be tolerated by the fish. For example, $\Omega\left(R/g\right)^{0.5} \approx 0.11$ for a typical cage with $R = 20$ m in the full scale, would lead to a maximum equilibrium flow velocity in the cage $U_{max} = R\Omega \approx 1.5$ m/s, and for $\Omega\left(R/g\right)^{0.5} \approx 0.45$, $U_{max} \approx 6$ m/s. The latter would be obviously too high compared to the critical swimming speed of fish (see, e.g., Hvas et al. 2020[2]), although the corresponding volume-averaged velocity in the whole cage would be somewhat lower than U_{max}. Thus, this sloshing suppression method can be practical only for fish cages with a relatively small radius (say $R < 10$ m).

Note that here we discussed a method for suppressing sloshing due to forced motion, i.e., in situations where the sloshing force does not significantly influence the cage motion. The latter is possible, e.g., if an integrated floating farm is considered, and its mass is much greater than the mass of the liquid contained in an individual closed unit. For a single cage, however, one may observe from Figure 8 that the added mass of the closed cage may be several times greater than the mass of the contained liquid ($\frac{F}{ma} > 1$ at $0.9 < f/f_1 < 1.3$). If this is the case for a floating closed cage exposed to sea waves, its motion in this frequency

range would be dominated by the added mass due to sloshing, and the cage response would be low if the total mass is great. Attempting to suppress sloshing waves in this case would decrease the added mass, naturally leading to an increased motion, and thus, the amplitude of the sloshing waves may not be reduced as intended.

V. CONCLUSIONS

Sloshing in an aquaculture closed-containment system with a slowly rotating liquid has been studied. It is found that the most important effect of the rotating flow is to split the natural frequencies of the non-rotating liquid, which leads to sloshing regimes that are not observed for the non-rotating liquid. It is shown that in the presence of rotation, transverse liquid oscillations causing swirling can be excited linearly in a wide range of frequencies. This contrasts with resonant sloshing in non-rotating liquids, where swirling is attributed to nonlinear effects as, e.g., near the lowest natural frequency f_1. Further, nonlinear resonant swirling regimes can also be observed in a rotating liquid; however, they occur near each of the pair frequencies split by rotation and not necessarily at f_1.

The violent sloshing that was observed in the non-rotating liquid at f_1 can be partly suppressed by rotation at sufficiently high angular velocities Ω (e.g., at $\Omega\,(R/g)^{0.5} > 0.11$ in our experiments). Relatively small cages (say $R < 10$ m) may benefit from this effect under forced-motion conditions. For larger cages, the same Ω would lead to flow velocities too high for fish. Lower Ω would not result in any significant sloshing suppression, as shown in our experiment at $\Omega\,(R/g)^{0.5} \approx 0.05$.

DATA AVAILABILITY

The data that support the findings of this study are available from the corresponding author upon reasonable request.

ACKNOWLEDGMENTS

This work was funded in part by the Research Council of Norway (grant no. 268402), the Norwegian Seafood Research Fund and all the industry partners of the project "Safe

operation of closed aquaculture cages in waves". C.L activity was supported by the Ministry of Science and Technology of P. R. China through Harbin Engineering University (G20190008061). C.L. was also supported by the Research Council of Norway through the Centers of Excellence funding scheme AMOS, project number 223254. Part of the activity of A.L. and C.L was funded also by the Italian Ministry of Economic Development under the Grant Agreement "RdS PTR 2019–2021 - Energia elettrica dal mare".

REFERENCES

[1]A. Nilsen, *Production of Atlantic salmon (Salmo salar) in closed confinement systems (CCS)-salmon lice, growth rates, mortality and fish welfare*, Ph.D. thesis, Norwegian University of life sciences (2019).

[2]M. Hvas, O. Folkedal, and F. Oppedal, "Fish welfare in offshore salmon aquaculture," Reviews in Aquaculture (2020).

[3]H. N. Abramson, W. H. Chu, and F. T. Dodge, "Nonlinear effects in lateral sloshing." Tech. Rep. (NASA TR SP-106, 1966) in: The Dynamic Behaviour of Liquids in Moving Containers.

[4]C. Lugni, M. Brocchini, and O. M. Faltinsen, "Wave impact loads: The role of the flip-through," PHYSICS OF FLUIDS **18** (2006), 10.1063/ 1.2399077.

[5]S. Malenica, L. Diebold, S. H. Kwon, and D.-S. Cho, "Sloshing assessment of the lng floating units with membrane type containment system where we are?" Marine Structures **56**, 99–116 (2017).

[6]C. Lugni, A. Bardazzi, O. M. Faltinsen, and G. Graziani, "Hydroelastic slamming response in the evolution of a flip-through event during shallow-liquid sloshing," Physics of Fluids **26** (2014), 10.1063/1.4868878.

[7]B. Bouscasse, M. Antuono, A. Colagrossi, and C. Lugni, "Numerical and experimental investigation of nonlinear shallow water sloshing," INTERNATIONAL JOURNAL OF NONLINEAR SCIENCES AND NUMERICAL SIMULATION **14**, 123–138 (2013).

[8]O. M. Faltinsen, O. F. Rognebakke, I. A. Lukovsky, and T. A. N, "Multidimensional modal analysis of nonlinear sloshing in a rectangular tank with finite water depth," Journal of Fluids Mechanics **407**, 201–234 (2000).

[9]O. M. Faltinsen, O. F. Rognebakke, and T. A. N, "Resonant three-dimensional nonlinear sloshing in a square-base basin. part 2. effect of higher modes," Journal of Fluids Mechanics **523**, 199–218 (2005).

[10]J. W. Miles, "Internally resonant surface waves in a circular cylinder," Journal of Fluid Mechanics **149**, 1–14 (1984).

[11]A. Royon-Lebeaud, E. J. Hopfinger, and A. Cartellier, "Liquid sloshing and wave breaking in circular and square-base cylindrical containers," Journal of Fluid Mechanics **577**, 467 (2007).

[12]O. M. Faltinsen, I. A. Lukovsky, and T. A. N, "Resonant sloshing in an upright annular tank," Journal of Fluids Mechanics **804**, 608–645 (2016).

[13]P. A. Caron, M. A. Cruchaga, and A. E. Larreteguy, "Study of 3d sloshing in a vertical cylindrical tank," PHYSICS OF FLUIDS **30** (2018), 10.1063/ 1.5043366.

[14]F. Dodge, *The New "dynamic Behavior of Liquids in Moving Containers"* (Southwest Research Inst., 2000).

[15]J. W. Miles, "Free surface oscillations in a rotating liquid," The Physics of Fluids **2**, 297–305 (1959).

[16]Y. Saito and T. Sawada, "Dynamic pressure change in a rotating, laterally oscillating cylindrical container," Journal of Ocean Engineering and Science **3**, 91 – 95 (2018).

[17]R. A. Ibrahim, *Liquid sloshing dynamics: theory and applications* (Cambridge University Press, 2005).

[18]I. M. Strand and O. M. Faltinsen, "Linear wave response of a 2d closed flexible fish cage," Journal of Fluids and Structures **87**, 58–83 (2019).

[19]Y. Tan, Y. Shao, and R. Read, "Coupled motion and sloshing analysis of a rigid cylindrical closed fish cage in regular waves," in *International Conference on Offshore Mechanics and Arctic Engineering*, Vol. 58837 (American Society of Mechanical Engineers, 2019) p. V006T05A005.

[20]I. M. Strand, *Sea loads on closed flexible fish cages*, Ph.D. thesis, Faculty of Engineering, Marine Technology Dept., NTNU (2018).

[21]D. Kristiansen, B. Su, and Z. Volent, "Numerical and experimental study on the drainage and collapse of a floating flexible bag structure," Journal of Fluids and Structures **83**, 429–447 (2018).

[22]P. Lader, D. W. Fredriksson, Z. Volent, J. DeCew, T. Rosten, and I. M. Strand, "Wave response of closed flexible bags," Journal of Offshore Mechanics and Arctic Engineering **139** (2017).

[23]P. Lader, D. W. Fredriksson, Z. Volent, J. DeCew, T. Rosten, and I. M. Strand, "Drag forces on, and deformation of, closed flexible bags," Journal of Offshore Mechanics and Arctic Engineering **137** (2015).

[24]O. M. Faltinsen and A. N. Timokha, *Sloshing*, Vol. 577 (Cambridge university press Cambridge, 2009).

[25]D. R. Plew, P. Klebert, T. W. Rosten, S. Aspaas, and J. Birkevold, "Changes to flow and turbulence caused by different concentrations of fish in a circular tank," Journal of Hydraulic Research **53**, 364–383 (2015).

[26]M. Antuono and C. Lugni, "Global force and moment in rectangular tanks through a modal method for wave sloshing," Journal of Fluids and Structures **77**, 1–18 (2018).